

# CD134 is a cellular receptor specific for human herpesvirus-6B entry

Huamin Tang<sup>a,b</sup>, Satoshi Serada<sup>c</sup>, Akiko Kawabata<sup>a,b</sup>, Megumi Ota<sup>a,b</sup>, Emi Hayashi<sup>b</sup>, Tetsuji Naka<sup>c</sup>, Koichi Yamanishi<sup>d</sup>, and Yasuko Morio<sup>a,b,1</sup>

<sup>a</sup>Division of Clinical Virology, Center for Infectious Diseases, Kobe University Graduate School of Medicine, Kobe 650-0017, Japan; and Laboratories of <sup>b</sup>Virology and Vaccinology and <sup>c</sup>Immune Signal, Division of Biomedical Research, <sup>d</sup>National Institute of Biomedical Innovation, Osaka 567-0085, Japan

Edited\* by Bernard Roizman, University of Chicago, Chicago, IL, and approved April 24, 2013 (received for review March 20, 2013)

Human herpesvirus-6B (HHV-6B) is a T lymphotropic  $\beta$ -herpesvirus that is clearly distinct from human herpesvirus-6A (HHV-6A) according to molecular biological features. The International Committee on Taxonomy of Viruses recently classified HHV-6B as a separate species. The primary HHV-6B infection causes exanthem subitum and is sometimes associated with severe encephalopathy. More than 90% of the general population is infected with HHV-6B during childhood, and the virus remains throughout life as a latent infection. HHV-6B reactivation causes encephalitis in immunosuppressed patients. The cellular receptor for HHV-6A entry was identified as human CD46, but the receptor for HHV-6B has not been clear. Here we found that CD134, a member of the TNF receptor superfamily, functions as a specific entry receptor for HHV-6B. A T-cell line that is normally nonpermissive for HHV-6B infection became highly susceptible to infection when CD134 was overexpressed. CD134 was down-regulated in HHV-6B-infected T cells. Soluble CD134 interacted with the HHV-6B glycoprotein complex that serves as a viral ligand, which inhibited HHV-6B but not HHV-6A infection in target cells. The identification of CD134 as an HHV-6B specific entry receptor provides important insight into understanding HHV-6B entry and its pathogenesis.

viral entry | gQ1 | gQ2

Human herpesvirus-6B (HHV-6B) is a T lymphotropic  $\beta$ -herpesvirus (1) and is clearly distinct from human herpesvirus-6A (HHV-6A) according to their genetic and antigenic differences and their cell tropism (2–5). Recently the International Committee on Taxonomy of Viruses classified HHV-6B as a separate species. The primary HHV-6B infection causes exanthem subitum (6) and is sometimes associated with severe encephalopathy, whereas the diseases caused by HHV-6A are still unknown. More than 90% of the general population is infected with HHV-6B during childhood, and the virus remains throughout life as a latent infection (7). HHV-6B reactivation causes encephalitis in immunosuppressed patients. HHV-6B reactivation is also associated with drug-induced hypersensitivity syndrome, and recent studies have suggested that it could be related to the severity of this disease (8, 9).

HHV-6A can infect a broader variety of human cells than HHV-6B (10), although the homology between HHV-6A and -6B is almost 90% over their entire genome (11–13). Human CD46 has been shown to be a cellular receptor of HHV-6 (14), and its viral ligand is a glycoprotein (g) complex made up of viral glycoprotein H (gH)/glycoprotein L (gL)/glycoprotein Q1 (gQ1)/glycoprotein Q2 (gQ2) (15). However, the HHV-6A gH/gL/gQ1/gQ2 complex binds to its human cellular receptor, CD46, whereas the corresponding complex of HHV-6B does not bind to it (10, 15). Moreover, anti-CD46 antibody does not block HHV-6B infection into the cells, whereas it does HHV-6A infection, indicating that the cellular receptor exists specific for HHV-6B infection. Because HHV-6B remains as a lifelong latent infection in more than 90% of the population and causes severe disease, it is important to identify its specific cellular receptor.

Here we show that CD134, a member of the TNF receptor superfamily, functions as a specific entry receptor for HHV-6B. A T-cell line that is normally nonpermissive for HHV-6B infection became highly susceptible to infection when CD134 was overexpressed. CD134 was down-regulated in HHV-6B-infected T cells. Soluble CD134 interacted with the HHV-6B glycoprotein complex that serves as a viral ligand, which inhibited HHV-6B but not HHV-6A infection in target cells. The identification of CD134 as an HHV-6B entry receptor provides important insight into understanding HHV-6B entry and its pathogenesis and for finding new targets for antiviral drug development.

## Results

**Construction of Soluble Glycoprotein Complex That Is a Viral Ligand for the Cellular Receptor.** To search for candidate molecules for the HHV-6B receptor, we first prepared a soluble form of the HHV-6A or -6B gH/gL/gQ1/gQ2 complex, which is expressed on the viral envelope and acts as a viral ligand for the cellular receptor (15). One component of the complex, gH, is a type I membrane protein that retains the other molecules, gQ1, gQ2, and gL, on the membrane through its interaction with them. Therefore, to prepare the soluble gH/gL/gQ1/gQ2 complex, the transmembrane domain and cytoplasmic tail of gH were removed, and the ectodomain of gH was fused in-frame with Fc (the fragment crystallizable region of the human IgG1 antibody) and a His tag. The production of the soluble complex was confirmed by immunoblot analysis using antibodies for each component of the complex (Fig. S1A). Notably, the soluble HHV-6B gH/gL/gQ1/gQ2 complex efficiently bound to the Molt-3 cell line, which is permissive for HHV-6B infection (Fig. S1B), whereas it bound poorly to the SupT1 cell line, which is nonpermissive (Fig. S1B). In contrast, the soluble HHV-6A gH/gL/gQ1/gQ2 complex bound to both the Molt-3 and SupT1 cell lines (Fig. S1B), which both express CD46 on their cell surface.

**Identification of Cellular Receptor Specific for HHV-6B.** Next, to identify the cellular receptor for HHV-6B, we performed pull-down assays using the soluble HHV-6A or -6B gH/gL/gQ1/gQ2 complex and lysates of surface-biotinylated Molt-3 cells. As expected, the molecular masses of the streptavidin-labeled bands differed between HHV-6A and -6B (Fig. 1A). The band detected in the HHV-6A sample seemed to correspond to CD46, but the band in the HHV-6B sample did not (Fig. 1A). The corresponding band detected by silver staining was excised from the gel and subjected to LC-MS/MS analysis. The results identified CD134 as a candidate receptor molecule for HHV-6B.

Author contributions: H.T. and Y.M. designed research; H.T., S.S., A.K., M.O., E.H., T.N., and Y.M. performed research; H.T., K.Y., and Y.M. analyzed data; and H.T. and Y.M. wrote the paper.

The authors declare no conflict of interest.

\*This Direct Submission article had a prearranged editor.

<sup>1</sup>To whom correspondence should be addressed. E-mail: ymorio@med.kobe-u.ac.jp.

This article contains supporting information online at www.pnas.org/lookup/suppl/doi:10.1073/pnas.1305187110/-DCSupplemental.

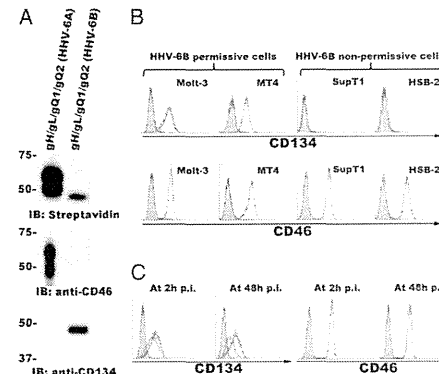


Fig. 1. CD134 interacts with HHV-6B gH/gL/gQ1/gQ2 and is expressed on HHV-6B permissive cells. (A) Purified HHV-6A or HHV-6B gH/gL/gQ1/gQ2 complex was incubated with the lysates from Molt-3 cells whose cell surface was labeled with EZ-link sulfo-NHS-Lc-Biotin. The complex and its binding proteins were immunoblotted and detected with streptavidin, anti-CD46, or anti-CD134 antibody. (B) CD134 or CD46 expression on HHV-6B permissive and nonpermissive cells. HHV-6B permissive (Molt-3 and MT4) or nonpermissive (SupT1, Jhhan, and HSB-2) cells were stained with anti-CD46 or CD134 antibody, followed by staining with secondary antibody for FACS analysis. Gray shading, isotype control. (C) Down-regulation of CD134 expression from the cell surface after HHV-6B infection. CD134 or CD46 expression on the surface of HHV-6B-infected Molt-3 cells was determined as described in B. Gray shading, isotype control; dark gray line, mock infection; light gray line, 2 h or 48 h postinfection (p.i.).

To confirm the identity of the corresponding band as CD134, immunoblotting was performed using the samples described above and an anti-CD134 antibody. The anti-CD134 antibody reacted with the eluate from the soluble HHV-6B gH/gL/gQ1/gQ2-bound resin but not with that from HHV-6A (Fig. 1A), indicating that CD134 associated specifically with the HHV-6B gH/gL/gQ1/gQ2 complex. On the other hand, an anti-CD46 antibody reacted with the eluate from the soluble HHV-6A gH/gL/gQ1/gQ2-bound resin but not with that from HHV-6B (Fig. 1A).

**Expression of CD134 in Several T-Cell Lines and Down-Regulation of CD134 on the Cell Surface by HHV-6B Infection.** HHV-6B permissive T-cell lines are distinct from those of HHV-6A. Therefore, next we assessed the level of CD134 protein expression in several T-cell lines by FACS analyses. CD134 was highly expressed in the HHV-6B permissive T-cell lines MT4 and Molt-3 but rarely in the HHV-6B nonpermissive T-cell lines HSB-2 and SupT1 (Fig. 1B). In contrast, CD46 was expressed abundantly in all of these cell lines (Fig. 1B).

In general the cellular receptor at the cell surface is down-regulated after viral infection. Therefore we examined the CD134 expression on the surface of HHV-6B-infected cells (Molt-3 cells). Fig. 1C shows that CD134 on the cell surface was down-regulated after HHV-6B infection, whereas the down-regulation of CD46 on the cell surface was rarely seen in the same condition.

**Inhibition of HHV-6B Infection by Soluble CD134 or Anti-CD134 Antibody.** Next we examined whether a soluble CD134Fc could inhibit HHV-6B infection of cells. HHV-6 entry into cells was examined by observing the expression of the HHV-6 immediate-early protein, IE1. As shown in Fig. 2, soluble CD134Fc blocked

HHV-6B (HST strain) infection in a dose-dependent manner, whereas neither soluble Fc nor soluble CD46Fc did so. Notably, soluble CD134Fc did not block HHV-6A infection, although soluble CD46Fc did block it (Fig. 2, Lower Left), indicating that CD134 functions as an HHV-6B-specific receptor but not as a receptor for HHV-6A. We further examined whether CD134 also functions as the receptor for the other HHV-6B strains (Z29 and KYO), including clinical isolates. The results showed that sCD134Fc could block the other HHV-6B strains tested (Fig. 2, Right), confirming that CD134 functions as a specific cellular receptor for HHV-6B isolates.

Furthermore, we analyzed whether the anti-CD134 antibody blocks HHV-6B infection into target cells. When MT4 cells were infected with HHV-6B in the presence of anti-CD134 antibody, infection was blocked by the anti-CD134 antibody (Fig. 3). By contrast, control antibody did not affect HHV-6B infection into the cells (Fig. 3).

**CD134-Expressing SupT1 Cells Become Susceptible for HHV-6B Infection.** Next, the CD134 gene was introduced into SupT1 cells, which are nonpermissive for HHV-6B infection, by a nonreplicative lentivirus, and HHV-6B was used to infect the CD134-overexpressing cells. The expression of CD134 on the SupT1 cells was confirmed by FACS (Fig. 4A). Notably, the CD134-expressing SupT1 cells were highly susceptible to HHV-6B entry (Fig. 4B), supporting the identification of CD134 as an HHV-6B receptor.

**Specific Interaction of HHV-6B Glycoprotein Complex and CD134.** HHV-6A and -6B share 90% identity in their nucleic acid sequence. However, the amino acid sequences of gQ1 and gQ2 show low identity, with 78% and 69%, respectively, between HHV-6A and -6B compared with the sequences of gH and gL (11–13). Therefore, the gQ1 and gQ2 components of the gH/gL/gQ1/gQ2 complex may contribute to the virus specificity for different cellular receptors. To examine this possibility, several chimeric complexes were expressed in 293T cells. The cell-surface expression of each component in the complexes was confirmed. The binding of soluble CD134Fc to the surface of these cells was then measured by FACS. No CD134Fc binding was detected when AgH/AgL/AgQ1/AgQ2 (Fig. 5A and C), AgH/AgL/BgQ1/AgQ2 (Fig. 5B and C), or BgH/BgL/AgQ1/AgQ2 (Fig. 5A and C) was expressed in 293T cells, whereas CD134Fc

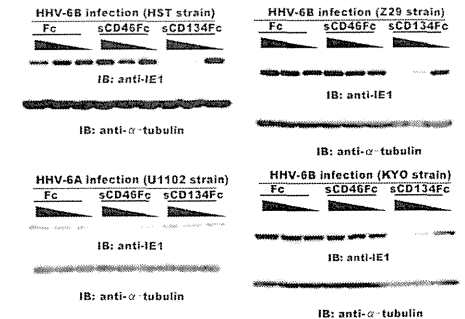
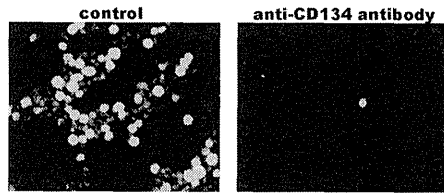


Fig. 2. CD134 is necessary for HHV-6B infection. HHV-6B (HST, KYO, or Z29 strain) or HHV-6A (U1102 strain) was incubated with the indicated amounts (diluted 10-fold from 2.5  $\mu$ g) of soluble CD134Fc, CD46Fc, or Fc, and then Molt-3 cells were infected with these viruses. The cell lysates were immunoblotted for HHV-6 immediate-early protein (IE1 or AIE1) and  $\alpha$ -tubulin.



**Fig. 3.** Anti-CD134 antibody blocks HHV-6B infection. MT4 cells were infected with HHV-6B in the presence of anti-CD134 antibody (guinea pig serum) or control antibody (preimmune serum). The infection was examined by indirect immunofluorescence antibody assay using BIE1 antibody.

bound to 293T cells expressing BgH/BgL/BgQ1/BgQ2 (Fig. 5 B and C) or AgH/AgL/BgQ1/BgQ2 (Fig. 5 B and C), indicating that CD134 specifically bound to complexes containing HHV-6B gQ1 and gQ2. These data suggest that gQ1 and gQ2 of HHV-6B but not of HHV-6A in the complex are essential for binding to CD134.

#### Discussion

Recently HHV-6B was classified as a separate species. Although its entry receptor has not been clear, here we found that CD134 is a cellular receptor specific for HHV-6B. Although HHV-6B and -6A share 90% identity in their nucleic acid sequence, they show distinct pathogenesis and cell tropism. The discovery of an HHV-6B-specific receptor supports the idea that the use of different receptors by HHV-6A and -6B is an important biological feature underlying their different characteristics and disease manifestations.

Previously we found that HHV-6A gH/gL/gQ1/gQ2 complex on the viral envelope is a viral ligand for CD46 (10, 16), which is a cellular receptor of HHV-6A (14). Here by using the soluble form of gH/gL/gQ1/gQ2 complex, we identified that the CD134 was a cellular receptor specific for HHV-6B. As predicted, the soluble form of HHV-6B gH/gL/gQ1/gQ2 complex bound to CD134, whereas that of HHV-6A did not. In addition, soluble CD134 could inhibit HHV-6B infection into target cells, whereas it could not inhibit HHV-6A infection, thus indicating that CD134 is a specific receptor for HHV-6B.

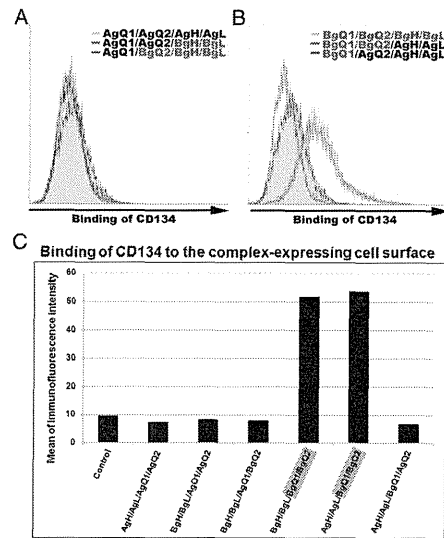


**Fig. 5.** HHV-6B-gQ1 and -gQ2 are the key molecules for HHV-6B's binding with CD134. (A and B) 293T cells were transfected with plasmids harboring individual molecules (indicated as different colors in histograms) or control plasmid (gray shading) and harvested 24 h later. The cells were incubated with soluble CD134Fc at 4 °C for 2 h and stained with Alexa Fluor 488 goat anti-human IgG antibody at 4 °C for 1 h for FACS analysis. (C) The intensity of immunofluorescence of the stained cells shown in A and B was quantified. A, HHV-6A; B, HHV-6B.

gQ1 and gQ2 in the complex are unique genes that are encoded specifically in HHV-6 and human herpesvirus-7 (HHV-7). In addition, HHV-6A and HHV-6B share low identity of them. Therefore we made several chimeric complexes of gQ1 and gQ2 and examined the interaction of chimeric complexes with CD134. Only the complex with HHV-6B gQ1 and gQ2 could bind to CD134, showing that gQ1 and gQ2 in the complex are crucial for the different receptor use between HHV-6B and HHV-6A.

CD134, which is also called OX40, is a member of the TNF receptor superfamily and is present on activated T lymphocytes, but it is rarely expressed on glial cells. HHV-6B is well known to have a cellular tropism for T lymphocytes, as shown in vivo during viremia from acute infection as well as in vitro (17, 18). Activated CD4<sup>+</sup> T lymphocytes are the preferential target of the fully permissive infection in vivo (18). Therefore, the present findings that strongly indicate CD134 is a functional HHV-6B entry receptor are consistent with the in vivo observations.

As described above, HHV-6B causes exanthem subitum in infants, and its reactivation causes encephalitis, especially in immunocompromised patients.

Because effective therapeutic agents for HHV-6B have not been developed, these findings may lead to new prophylactic and therapeutic approaches for HHV-6B-associated diseases, through the development of drugs that target CD134 and its regulators.

#### Materials and Methods

**Plasmids.** An Fc fragment of human IgG1 with L266A and L267E mutations to reduce its binding affinity to cellular Fc receptors was used (19). The IL-2 signal sequence (amplified from pFuse-hlg1-Fc2; InvivoGen) was used in

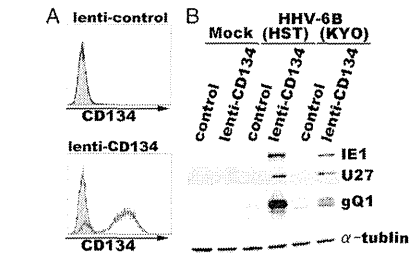


**Fig. 4.** SupT1 cells overexpressing CD134 become permissive for HHV-6B infection. (A) SupT1 cells were transfected with lentivirus or CD134-expressing lentivirus. CD134 expression on the SupT1 cells was confirmed by FACS analysis using an anti-CD134 antibody before HHV-6B infection. Gray shading, isotype control. (B) Four days later, the cells were infected with HHV-6B (HST or KYO strain), followed by immunoblotting with anti-HHV-6B IE1, -U27, -gQ1, and  $\alpha$ -tubulin antibodies.

Tang et al.

PNAS Early Edition | 3 of 4

place of the original signal sequence in each of the Fc fusion protein-expressing plasmids. In the CD46-expressing plasmid, the original signal sequence was used. To generate gHFcHis-expressing plasmids, the nucleic acid sequence for the ectodomain of gH (base pairs 46–2067) was amplified from the HHV-6A and -6B genomes by PCR, ligated with the Fc fragment containing a 6x histidine sequence at its 3' end, and cloned into the pCAGGS-MCS plasmid (20). Similarly, FcHis, CD46FcHis (base pairs 1–1029 of the CD46 sequence), and CD134FcHis (base pairs 85–642 of the CD134 sequence) were cloned into pCAGGS-MCS (provided by J. Miyazaki, Osaka University, Suita, Japan). We cloned the full-length CD134 sequence into CS-CA-MCS (provided by RIKEN: the Institute of Physical and Chemical Research; Japan) plasmid. The plasmids for expressing gQ1, gQ2, gH, and gL of HHV-6A and -6B were described previously (21, 22).

**Antibodies.** Mouse monoclonal antibodies to CD46 (J4, 48) and CD134 (Ber-ACT35) were purchased from Immunotech and BioLegend, respectively. The antibodies to IE1, U27, gH/gL, gH, gQ1, and gQ2 of HHV-6A and HHV-6B were described previously (21–23). Anti-CD134 antibody was obtained by immunizing the purified CD134 protein to guinea pigs. Preimmune sera of guinea pigs were used as control antibody.

**Fc-Fusion Protein.** The plasmids for expressing Fc-fusion proteins were transfected into 293T cells using Lipofectamine 2000 (Invitrogen), according to the manufacturer's instructions. Two days after transfection, the soluble Fc-fusion proteins in the culture medium were purified by Ni-NTA (Qiagen) affinity chromatography.

**Identification of Proteins Associated with the BgH/BgL/BgQ1/BgQ2 Complex.** 293T cells were transfected with BgH/FcHis, BgL-, BgQ1-, and BgQ2-expressing plasmids or with AgH/FcHis, AgL-, AgQ1-, and AgQ2-expressing plasmids. The culture medium was harvested 48 h after transfection, incubated with Ni-NTA at 4 °C for 8 h, and then the Ni-NTA was spun down. Molt-3 cells (T-cell line) ( $1 \times 10^6$  cells per sample) were labeled with EZ-link sulfo-NHS-LC-Biotin (Thermo Scientific) according to the manufacturer's protocol and lysed with TNE buffer [10 mM Tris-HCl (pH 7.8), 0.15 M NaCl, 1 mM EDTA, and 1% Nonidet P-40 (Nacal Tesque)]. After centrifugation, the supernatant was incubated with the glycoprotein complex-bound Ni-NTA described above at 4 °C for 16 h. The proteins that bound to the Ni-NTA were eluted with 250 mM imidazole, and the buffer was changed to PBS using centrifugal filter devices (Millipore). Finally, the protein solution was incubated with protein G Sepharose at 4 °C for 8 h. The eluates were prepared for immunoblot analysis [using streptavidin-HRP (GE Healthcare) and silver staining (Invitrogen)]. The positive bands in the silver-stained gel (corresponding to the position of the positive band in the Western blot) were excised for in-gel digestion and LC-MS/MS analysis (24).

**Preparation of Virus Solution.** To prepare virus stocks, the viruses (HHV-6A and -6B strains) were propagated in umbilical cord blood mononuclear cells (CBMCs) provided by K. Adachi (Minoh Hospital, Minoh, Japan) and H. Yamada (Kobe University Graduate School of Medicine, Kobe, Japan) and purchased from the Cell Bank of the RIKEN Bioresource Center, which had been stimulated with 5  $\mu$ g/mL phytohemagglutinin and 2 ng/mL IL-2 for 3 d. When more than 80% of the cells showed cytopathic effects, the cultures were frozen and thawed twice, then centrifuged at 1,500  $\times$  g for 5 min. The supernatants were collected and stored at -80 °C as cell-free virus stocks. We used CBMCs to titrate the viruses by the 50% tissue culture infectious dose assay (25).

**Infection Inhibition Assay.** Cell-free HHV-6A or HHV-6B virus was incubated with soluble Fc, CD46Fc, or CD134Fc (diluted 10-fold from 2.5  $\mu$ g) at 37 °C for 30 min, and then the virus was used to infect Molt-3 cells ( $5 \times 10^5$ ) at 37 °C for 1 h. The cells were cultured in 1 mL of medium for 24 h and then lysed with RIPA buffer [50 mM Tris (pH 7.4), 150 mM EDTA, 1% Triton X-100, 1% sodium deoxycholate, and 0.1% SDS] and used for immunoblotting analysis.

**Cell-Surface Expression Assay.** Cells were incubated with isotype control, anti-CD46, or anti-CD134 antibody at 4 °C for 1 h, followed by a secondary antibody. The cells were fixed with 4% (wt/vol) paraformaldehyde for 10 min before being analyzed on a FACSCalibur (BD).

**Cell-Surface Binding Assay.** Fc or soluble Fc-fusion proteins were incubated with a T-cell line (Molt-3 or SupT1) or with 293T cells transfected with glycoprotein-expressing plasmids (24 h after transfection) at 4 °C for 2 h, then the cells were washed with 3% (wt/vol) BSA/PBS and stained with an Alexa Fluor 488 goat anti-human IgG antibody (Invitrogen) at 4 °C for 1 h. The cells were washed with PBS, fixed with 4% (wt/vol) paraformaldehyde for 10 min, and then subjected to FACS analysis.

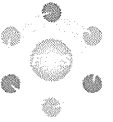
**Overexpression of CD134 in SupT1 Cells and Infection with HHV-6B.** CD134-expressing lentivirus and its control were constructed by transfecting 293T cells with CS-CA-MCS-CD134 (or its control, CS-CA-MCS) and packaging plasmids (pCAG-HIV-gag and pCMV-VSV-G-RSV-Rev provided by RIKEN). The culture media containing the viruses were harvested 3 d after transfection. SupT1 cells were transfected with the lentiviruses for 4 d and then infected with HHV-6B viruses. The cells were harvested and prepared for immunoblot analysis.

**ACKNOWLEDGMENTS.** We thank Y. Yamamoto (National Institute of Biomedical Innovation) and E. Moriishi (National Institute of Biomedical Innovation) for technical assistance. J. Miyazaki (Osaka University) for providing reagents, and K. Adachi (Minoh City Hospital) and H. Yamada (Kobe University) for the CBMCs. This work was supported by a Grant-in-Aid for Scientific Research (B) from the Japan Society for the Promotion of Science.

- Roizmann B, et al. (1999) The Herpesvirus Study Group of the International Committee on Taxonomy of Viruses (1992) The family Herpesviridae: An update. *Arch Virol* 123(3-4): 425-449.
- Salahuddin SZ, et al. (1986) Isolation of a new virus, HBLV, in patients with lymphoproliferative disorders. *Science* 234(4776):596-601.
- Aubin JT, et al. (1991) Several groups among human herpesvirus 6 strains can be distinguished by Southern blotting and polymerase chain reaction. *J Clin Microbiol* 29(2):367-372.
- Campadelli-Fiume G, Guerrini S, Liu X, Foà-Tomasi L (1993) Monoclonal antibodies to glycoprotein B differentiate human herpesvirus 6 into two clusters, variants A and B. *J Gen Virol* 74(9):2257-2262.
- Wyatt LS, Balachandran N, Frenkel N (1990) Variations in the replication and antigenic properties of human herpesvirus 6 strains. *J Infect Dis* 162(4):852-857.
- Yamanishi K, et al. (1988) Identification of human herpesvirus-6 as a causal agent for exanthem subitum. *Lancet* (8594):1065-1067.
- Okuno T, et al. (1989) Seroepidemiology of human herpesvirus 6 infection in normal children and adults. *J Clin Microbiol* 27(4):651-653.
- Pritchett JC, Nanau RM, Neuman MG (2012) The link between hypersensitivity syndrome reaction development and human herpes virus-6 reactivation. *Int J Hepatol* 2012:23062.
- Tahiyama M, et al. (2007) Association of human herpesvirus 6 reactivation with the flaring and severity of drug-induced hypersensitivity syndrome. *Br J Dermatol* 157(5): 934-940.
- Mori Y (2009) Recent topics related to human herpesvirus 6 cell tropism. *Cell Microbiol* 11(7):1001-1006.
- Dominguez G, et al. (1999) Human herpesvirus 6B genome sequence: Coding content and comparison with human herpesvirus 6A. *J Virol* 73(10):8040-8052.
- Gompels UA, et al. (1995) The DNA sequence of human herpesvirus-6: Structure, coding content, and genome evolution. *Virology* 209(1):29-51.
- Isegawa Y, et al. (1999) Comparison of the complete DNA sequences of human herpesvirus 6 variants A and B. *J Virol* 73(10):8053-8063.
- Santoro F, et al. (1999) CD46 is a cellular receptor for human herpesvirus 6. *Cell* 99(7): 817-827.
- Akkapaboon P, Mori Y, Sadaoka T, Yonemoto S, Yamanishi K (2004) Intracellular processing of human herpesvirus 6 Q1 and Q2 into tetrameric complexes expressed on the viral envelope. *J Virol* 78(15):7969-7983.
- Mori Y, et al. (2004) Discovery of a second form of tripartite complex containing gH-gL of human herpesvirus 6 and observations on CD46. *J Virol* 78(9):4609-4616.
- Ablashi DV, et al. (1991) Genomic polymorphism, growth properties, and immunologic variations in human herpesvirus-6 isolates. *Virology* 184(2):545-552.
- Takahashi K, et al. (1989) Predominant CD4 T-lymphocyte tropism of human herpesvirus 6-related virus. *J Virol* 63(7):3161-3163.
- Shiratori I, Ogasawara K, Saito T, Lamer LL, Arase H (2004) Activation of natural killer cells and dendritic cells upon recognition of a novel CD99-like ligand by paired immunoglobulin-like type 2 receptor. *J Exp Med* 199(4):525-533.
- Niwa H, Yamamura K, Miyazaki J (1991) Efficient selection for high-expression transfectants with a novel eukaryotic vector. *Gene* 108(2):193-199.
- Kawabata A, et al. (2011) Analysis of a neutralizing antibody for human herpesvirus 6B reveals a role for glycoprotein Q1 in viral entry. *J Virol* 85(24):12962-12971.
- Tang H, Hayashi M, Maeki T, Yamanishi K, Mori Y (2011) Human herpesvirus 6 glycoprotein complex formation is required for folding and trafficking of the gH/gL/gQ1/gQ2 complex and its cellular receptor binding. *J Virol* 85(21):11121-11130.
- Mori Y, et al. (2002) Human herpesvirus 6 variant A B2 but not variant B induces fusion from without in a variety of human cells through a human herpesvirus 6 entry receptor, CD46. *J Virol* 76(13):6750-6761.
- Shevchenko A, Wilm M, Vorm O, Mann M (1996) Mass spectrometric sequencing of proteins silver-stained polyacrylamide gels. *Anal Chem* 68(3):850-858.
- Asada H, Yalcin S, Balachandran K, Higashi K, Yamanishi K (1989) Establishment of titration system for human herpesvirus 6 and evaluation of neutralizing antibody response to the virus. *J Clin Microbiol* 27(10):2204-2207.

4 of 4 | www.pnas.org/cgi/doi/10.1073/pnas.1305187110

Tang et al.



# Supporting Information

Tang et al. 10.1073/pnas.1305187110

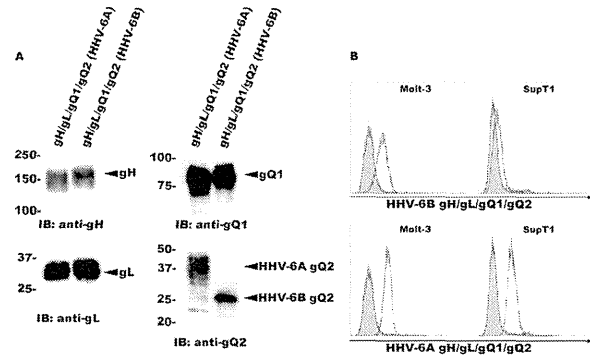


**Fig. S1.** Specific binding of soluble HHV-6B gH/gL/gQ1/gQ2 complex to virus permissive cells. (A) Secretion of the AgHFd/AgL/AgQ1/AgQ2 or BgHFd/BgL/BgQ1/BgQ2 complex. 293T cells were cotransfected with several plasmids harboring individual molecules. The culture medium was harvested 2 d after transfection, and the recombinant proteins were purified by Ni-NTA affinity chromatography and subjected to immunoblot analysis using antibodies for each component of the complex. (B) The HHV-6B ligand binds to Molt-3 (HHV-6B permissive) but not SupT1 (HHV-6B nonpermissive) cells. Molt-3 (HHV-6B permissive) or SupT1 (HHV-6B nonpermissive) cells were incubated with soluble HHV-6A- or HHV-6B gHFd/gL/gQ1/gQ2 complex at 4 °C for 2 h, stained with Alexa Fluor 488 goat anti-human IgG antibody at 4 °C for 1 h, and subjected to FACS analysis. Gray shading, incubated with Fc as control.

## Calretinin mediates apoptosis in small cell lung cancer cells expressing tetraspanin CD9\*

Ping He<sup>a,c,1</sup>, Hanako Kuhara<sup>a,1</sup>, Isao Tachibana<sup>a,1</sup>, Yingji Jin<sup>a</sup>, Yoshito Takeda<sup>a</sup>, Satoshi Tetsumoto<sup>a</sup>, Toshiyuki Minami<sup>a</sup>, Satoshi Kohmo<sup>a</sup>, Haruhiko Hirata<sup>a</sup>, Ryo Takahashi<sup>a</sup>, Koji Inoue<sup>a</sup>, Izumi Nagatomo<sup>a</sup>, Hiroshi Kida<sup>a</sup>, Takashi Kijima<sup>a</sup>, Tetsuji Naka<sup>a,d</sup>, Eiichi Morii<sup>b</sup>, Ichiro Kawase<sup>a</sup>, Atsushi Kumanogoh<sup>a,e</sup>

<sup>a</sup>Department of Respiratory Medicine, Allergy and Rheumatic Diseases, Osaka University Graduate School of Medicine, Osaka 565-0871, Japan

<sup>b</sup>Department of Pathology, Osaka University Graduate School of Medicine, Osaka 565-0871, Japan

<sup>c</sup>Department of Respiratory Medicine, The Second Affiliated Hospital, School of Medicine, Xi'an Jiaotong University, Xi'an 71004, China

<sup>d</sup>Laboratory of Immune Signal, National Institute of Biomedical Innovation, Osaka 567-0085, Japan

<sup>e</sup>CREST, JST, Department of Immunopathology, WPI Immunology Frontier Research Center, Osaka University, Osaka 565-0871, Japan

### ARTICLE INFO

#### Article history:

Received 17 January 2013

Received in revised form 5 April 2013

Accepted 26 April 2013

#### Keywords:

Small cell lung cancer  
Proteomics  
Tetraspanin  
CD9  
Calretinin  
Apoptosis

### ABSTRACT

A majority of small cell lung cancer (SCLC) cells lack a metastasis suppressor, tetraspanin CD9, and CD9 expression promotes their apoptosis. By a proteomics-based approach, we compared an SCLC cell line with its CD9 transfectant and found that a calcein-binding neuronal protein, calretinin, is upregulated in CD9-positive SCLC cells. Ectopic or anticancer drug-induced CD9 expression upregulated calretinin, whereas CD9 knockdown down-regulated calretinin in SCLC cells. When calretinin was knocked down, CD9-positive SCLC cells revealed increased Akt phosphorylation and decreased apoptosis. These results suggest that CD9 positively regulates the expression of calretinin that mediates proapoptotic effect in SCLC cells.

© 2013 The Authors. Published by Elsevier B.V. on behalf of Federation of European Biochemical Societies. All rights reserved.

### 1. Introduction

Small cell lung cancer (SCLC) is highly malignant lung tumor that spreads early throughout the body. It is characterized by neuroendocrine features such as neuropeptide production and N-CAM expression [1]. At diagnosis in most cases, SCLC has already metastasized to regional lymph nodes and distant organs including brain, bone, liver, and adrenal gland, thus excluding the possibility of surgical resection. Currently, standard treatment against extended SCLC is chemotherapy including cisplatin and etoposide [2]. Despite its high sensitivity to these anticancer drugs, SCLC rapidly develops recurrent tumors locally and at the distant organs. Such malignant phenotype is at least partially caused by acquired resistance to apoptotic cell death [3]. Elucidation of its mechanisms is necessary to improve outcome

of chemotherapy, but little has been clarified.

Tetraspanins are a family of membranous proteins that has characteristic structure spanning the membrane four times. Through association with other functional proteins including integrins, growth factor receptors, membrane proteases, and intracellular signaling molecules, tetraspanins organize multiprotein complexes at the tetraspanin-enriched microdomain (TEM) and regulate cell adhesion, migration, and survival [4,5]. Among 33 members in humans, CD9 and CD82 are known as a metastasis suppressor of solid tumors. Clinical and pathological findings suggest that decreased expressions of these tetraspanins are associated with progression of cancers of breast, pancreas, colon, and esophagus, and nonsmall cell lung cancer (NSCLC) and thus with poor prognosis [6,7].

We have shown that, among tetraspanins, CD9 is selectively absent in a majority of SCLC lines and SCLC tissues in contrast to NSCLC which frequently expresses CD9, and that ectopic expression of CD9 in SCLC cells suppresses integrin  $\beta 1$ -dependent cell motility [8] and promotes apoptotic cell death through attenuation of PI3K/Akt signaling [9]. These results suggest that the absence of CD9 contributes to highly malignant phenotype of SCLC. We also found that CD9 expression is induced and cell motility is decreased when SCLC cells are exposed to cisplatin or etoposide [10]. In the present study, we compared an SCLC cell line with its CD9 transfectant by a proteomics-based approach and found that a calcium-binding neuronal protein,

\* This is an open-access article distributed under the terms of the Creative Commons Attribution License, which permits unrestricted use, distribution, and reproduction in any medium, provided the original author and source are credited.

Abbreviations: SCLC, small cell lung cancer; NSCLC, nonsmall cell lung cancer; PARP, poly(ADP-ribose)polymerase; PMF, peptide mass fingerprinting; MALDI-TOF, matrix-assisted laser desorption/ionization time-of-flight; RT-PCR, reverse transcription-PCR; KO, knockout

<sup>1</sup> These authors contributed equally to the study.

\* Corresponding author. Tel.: +81 6 6879 3833; fax: +81 6 6879 3839.

E-mail address: itachi02@imed3.med.osaka-u.ac.jp (I. Tachibana).

calretinin, is upregulated in CD9-positive SCLC cells. We also show that calretinin mediates apoptotic cell death of SCLC.

## 2. Materials and methods

### 2.1. Cell lines

OS1, OS2-RA, and OS3-R5 were SCLC cell lines established in our laboratory, and their biological properties were previously characterized [8]. SCLC lines, OC10 and CADO LCG, a lung adenocarcinoma cell line, CADO LCG, and a mesothelioma cell line, OC-(MT)37, were provided by Osaka Medical Center for Cancer and Cardiovascular Diseases (Osaka, Japan) [11]. An SCLC line, SBC-3, and its chemoresistant sub-line, SBC-3/CDDP, were kindly provided by Dr. K. Kiura (Okayama University, Okayama, Japan) [10]. SCLC cell lines, NCI-H69, NCI-N231, and NCI-H209, a lung adenocarcinoma line, A549, and pleural mesothelioma lines, NCI-H226, NCI-H2452, NCI-H28, and MSTO-211H, were purchased from American Type Culture Collection (Rockville, MD). A lung squamous cell carcinoma line, HARA, was a kind gift from Dr. H. Iguchi (Kyusyu Cancer Center, Fukuoka, Japan). All cell lines were maintained in RPMI 1640 medium supplemented with 10% heat-inactivated FBS, 100 U/ml penicillin, and 100 µg/ml streptomycin.

### 2.2. Antibodies and reagents

Mouse anti-CD9 mAb (MM2/57), anti-poly(ADP-ribose)polymerase (PARP) mAb (42/PARP), and anti-β-actin mAb (C4) were purchased from Biosource, BD Biosciences, and Santa Cruz Biotechnology, respectively. Mouse anti-CD9 mAb (72F6) was purchased from Novocastra. Goat anti-calretinin polyclonal Ab (AB1550) and rabbit anti-calretinin polyclonal Ab (DC8) were purchased from Chemicon International and Zymed Laboratories, respectively. Rabbit anti-cleaved PARP (Asp214) mAb (D64E10), anti-phospho-Akt (Ser473) mAb (D9E), and anti-Akt polyclonal Ab were purchased from Cell Signaling Technology. Cisplatin (CDDP) was provided by Nippon Kayaku Co. (Tokyo, Japan).

### 2.3. Flow cytometry

Cells (10<sup>4</sup>) were incubated with 10 µg/ml primary mouse mAbs and labeled with FITC-conjugated goat anti-mouse immunoglobulin (Biosource International). Normal mouse IgG was used as a control. Stained cells were analyzed on a FACScan (Becton Dickinson).

### 2.4. cDNA and small interfering RNA (siRNA) transfection

Establishment of stable CD9-, NAG-2-, and mock-transfectants of OS3-R5 was previously described [8,9]. Cells were transfected with 40 nM cocktail siRNAs against human CD9 (No. SHF27A-0631; B-Bridge International) or human calretinin (No. SHF27A-0981; B-Bridge International), or negative control cocktail RNAs (No. S30C-0126; B-Bridge International) using LipofectAMINE 2000 Reagent (Invitrogen).

### 2.5. Two-dimensional electrophoresis (2-DE) and mass spectrometry analysis

Proteins were extracted from cells with the Complete Mammalian Proteome Extraction Kit (Calbiochem, Darmstadt, Germany). For 2-DE, isoelectric focusing (IEF) was performed using the PROTEAN IEF cell (Bio-Rad laboratories) according to the manufacturer's instructions. Extracted proteins were reconstituted in a rehydration buffer (7 M urea, 2 M thiourea, 4% CHAPS, 2 mM tributylphosphine (TBP), 0.0002% bromophenol blue (BFB), 0.2% Bio-lyte ampholyte 4–7) and applied to ReadyStrip™ IPG strips (11 cm, pH 4–7). IEF was run for 45,000 Vh. Two-dimensional electrophoresis was carried out in 10% Bis-Tris Criterion™ XT Precast gels. After staining with the Silver

Stain MS Kit (Wako Pure Chemical Industries, Osaka, Japan), the gels were captured by transmission scanning and analyzed with Image Master 5.0 (Amersham Biosciences). Following analysis, selected protein spots were manually excised from the gels and digested with trypsin (Promega) according to published procedures [12]. All peptide mass fingerprinting (PMF) spectra were obtained by using an ultraflex TOF/TOF matrix-assisted laser desorption/ionization time-of-flight (MALDI-TOF) mass spectrometer (Bruker Daltonics, Bremen, Germany).

### 2.6. Database search

PMF data were searched with Mascot software (Matrix Science, London, UK) against NCBI or Swiss-Prot databases. Protein database searching was performed with following parameters: *Homo sapiens*, maximum of one missed, cleavage by trypsin, monoisotopic mass value, charge state of 1+, allowing a mass tolerance of 100 ppm, and carbamidomethyl modification of cysteine. Protein scores of >64 indicate identity or extensive homology ( $P < 0.05$ ) and were considered significant.

### 2.7. Reverse transcription-PCR (RT-PCR)

One microgram of total RNA was reversely transcribed with a cDNA synthesis kit (Invitrogen) using random hexamers. The thermal cycling parameters were 30 cycles of 40 s at 94 °C, 40 s at 60 °C, and 90 s at 72 °C for CD9 and 30 cycles of 30 s at 94 °C, 30 s at 60 °C, and 90 s at 72 °C for calretinin. We confirmed that these variables yielded amplification of template DNAs within a linear range. The sequences of upstream and downstream oligonucleotide primers for CD9 was previously described [8]. Upstream and downstream oligonucleotide primers used for calretinin were 5'-GGAAGCACTTTGACGACAGC-3' and 5'-CTCGCTGACAGACAATCTC-3', respectively.

### 2.8. Immunoprecipitation and immunoblotting

Cells were lysed in lysis buffer containing 1% Brij 99, 25 mM HEPES, pH 7.5, 150 mM NaCl, 5 mM MgCl<sub>2</sub>, 2 mM phenylmethylsulfonyl fluoride, 10 µg/ml aprotinin, and 10 µg/ml leupeptin. Whole cell lysates or immunoprecipitates with anti-CD9 mAb (MM2/57) were separated by 10% SDS-PAGE under nonreducing conditions for CD9 or under reducing conditions for the other proteins. After transfer to Immobilon-P membranes (Millipore), immunoblotting was performed with primary Abs followed by peroxidase-conjugated secondary Abs. Immunoreactive bands were visualized with a chemiluminescent reagent (PerkinElmer).

### 2.9. Immunohistochemistry

A human SCLC tissue array was purchased from US Biomax Inc. It contained small cell carcinoma tissues from 30 individuals and normal tissues from three individuals. Each specimen was represented by two cores from different tissue spots. After antigen retrieval, inactivation of endogenous peroxidase, and blockade of non-specific reaction, the tissue microarray sections were stained with anti-CD9 mAb (72F6) or anti-calretinin Ab (DC8), followed by incubation with biotinylated goat anti-mouse and rabbit IgG Ab and streptavidin-conjugated peroxidase. These were counterstained with Mayer's hematoxylin [10]. Specimens were regarded as positive when staining was observed in more than 30% of tumor cells on average. The significance of association between CD9 staining and calretinin staining was evaluated by Fisher's exact test.

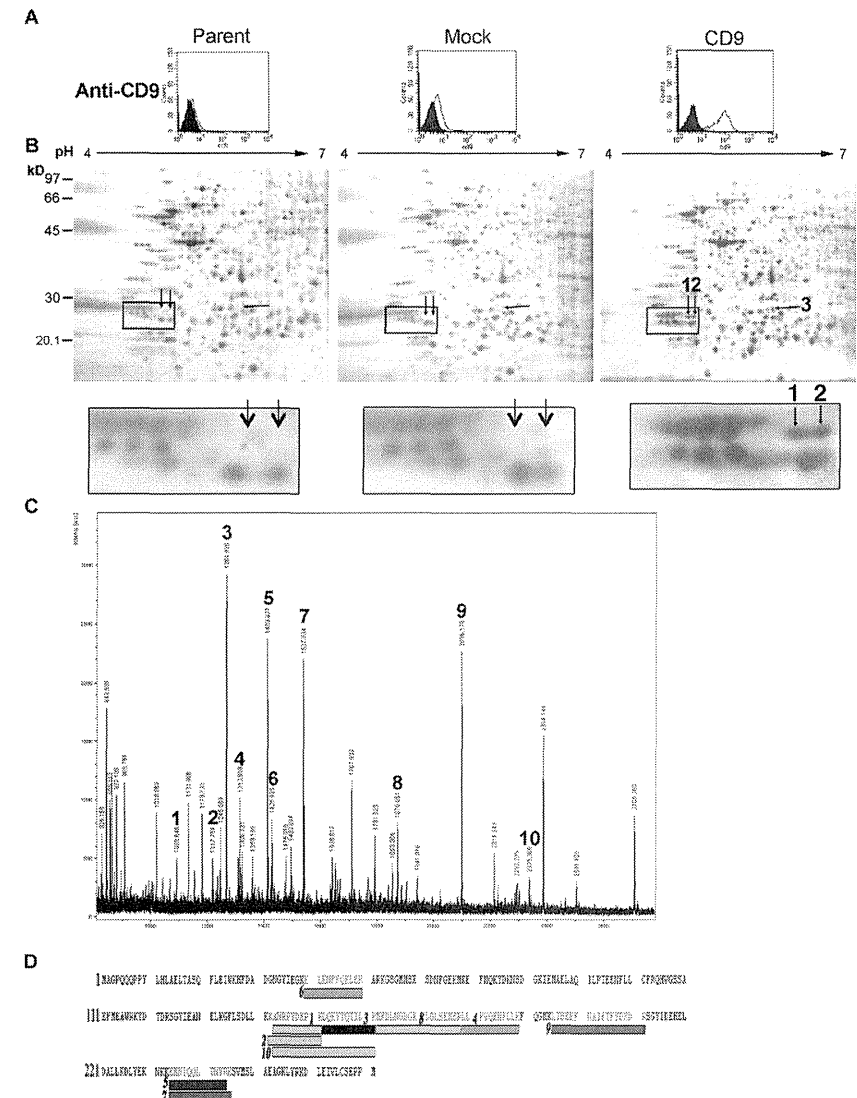


**Fig. 1.** Comparative proteomic analysis of the parent and CD9-overexpressing SCLC cells. (A) The parent, mock transfectant, and CD9 transfectant of OS3-R5 were stained with anti-CD9 mAb, labeled with FITC-conjugated goat anti-mouse immunoglobulin, and analyzed on a FACScan (Open histograms). Closed histograms indicate staining with control IgG. (B) Representative 2-DE maps of OS3-R5 and its transfectants. Arrows 1–3 indicate protein spots selectively identified in OS3-R5-CD9 by mass spectrometry. 1 and 2, calretinin; 3, PA28 $\alpha$ . Images including the calretinin spots were enlarged in lower columns. (C) PMF spectra of spot 2 obtained by MALDI-TOF. Mass peaks, peptides of which were matched with human calretinin, are marked with numbers. (D) The matched peptides in panel (C) were indicated with bars, yielding 33% sequence coverage of calretinin.

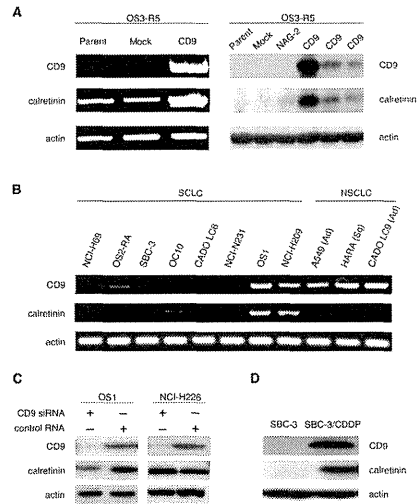


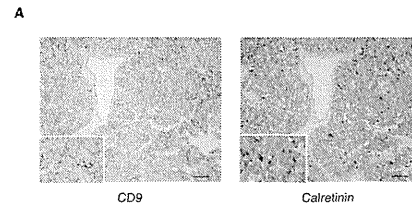
**Fig. 2.** Co-expression of CD9 and calretinin in SCLC cells. (A) Total RNA was extracted from the parent, mock transfected, and CD9 transfected of OS3-R5 and analyzed for expressions of CD9 and calretinin by RT-PCR.  $\beta$ -Actin amplification was used as the internal control (left). The parent, mock transfected, NAG-2 transfected, and CD9 transfected of OS3-R5 were lysed with 1% Brij 99 lysis buffer. Cell lysates were analyzed for expressions of CD9 and calretinin by immunoblotting. Anti- $\beta$ -actin blots were used as the internal control (right). (B) Total RNA was extracted from multiple SCLC and NSCLC cell lines and analyzed for expressions of CD9 and calretinin by RT-PCR. Ad, adenocarcinoma; Sq, squamous cell carcinoma. (C) An SCLC line OS1 (left) or a mesothelioma line NCI-H226 (right) was transfected with siRNAs against CD9 or control RNAs. Cell lysates were analyzed for expressions of CD9 and calretinin by immunoblotting. (D) Cell lysates of SCLC lines SBC-3 and SBC-3/CDDP were analyzed for expressions of CD9 and calretinin by immunoblotting.

## 2.10. Mice

The generation of CD9 knockout (KO) mice was described previously [13]. These mice were backcrossed more than six generations into the C57BL/6J background. The mice were bred in a barrier facility, and all animal procedures were performed in accordance with the Osaka University guidelines on animal care.

## 2.11. Apoptosis analysis

Cells were transfected with siRNA against calretinin or negative control RNAs. After 24 h, the cells were cultured in the absence or presence of CDDP in low-serum (0.1% FBS) RPMI 1640 for 48 h. Apoptotic cleavage of PARP [14] and decrease of Akt phosphorylation [9] were analyzed by immunoblotting. Viable cells were quantified with Cell Counting Kit-8 (Dojindo Laboratories, Kumamoto, Japan). Assays were performed in triplicate cultures and values are expressed as mean  $\pm$  SD. Statistical differences were determined by Student's *t*-test.  $P < 0.05$  was considered statistically significant.



	calretinin	
	positive	negative
CD9	7 (23.3%)	4 (13.3%)
negative	4 (13.3%)	15 (50.0%)

$P=0.047$

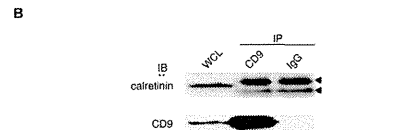


**Fig. 3.** CD9 is not physically associated with calretinin. (A) Immunohistochemical staining of CD9 and calretinin in a double-positive specimen from an SCLC tissue microarray. Insets show enlarged images of a part of sections. Bar, 50  $\mu$ m. Significant association between CD9 and calretinin expressions in the tissue microarray was evaluated by Fisher's exact test (table). (B) CD9 and calretinin in whole cell lysate (WCL) and in immunoprecipitates (IP) with anti-CD9 mAb or control IgG of OS3-R5-CD9 were immunoblotted (IB). Arrowheads indicate nonspecific binding of secondary Abs.

## 3. Results

### 3.1. Identification of proteins upregulated in OS3-R5-CD9 cells

We previously established a CD9 (-) SCLC cell line OS3-R5 and its CD9 transfected OS3-R5-CD9 and revealed that the CD9 transfected cells were less motile on fibronectin [8] and revealed enhanced apoptosis in low-serum culture conditions [9]. To detect molecules that regulate these changes, cell lysates of the parent, mock transfected, and CD9 transfected of OS3-R5 (Fig. 1A) were subjected to 2-DE, and protein spots were visualized by silver stain of the gels. Spots selectively overexpressed in OS3-R5-CD9 were identified (Fig. 1B) and the corresponding proteins were analyzed by mass spectrometry. We repeated this experiment and found that two proteins, a calcium-binding protein, calretinin, and a proteasome activator subunit 1, PA28 $\alpha$ , were reproducibly overexpressed in OS3-R5-CD9 cells (Table S1). Fig. 1C shows PMF spectra of spot 2 obtained by MALDI-TOF. Matched peptides were found to cover 33% of protein sequence of calretinin (Fig. 1D). Based on the fact that SCLC has neuronal features, we further analyzed calretinin, which is a protein distributed in the nervous system.

### 3.2. Co-expression of CD9 and calretinin in SCLC cells

RT-PCR revealed that the calretinin gene was minimally transcribed in the parent and mock-transfected OS3-R5 cells, and that ectopic expression of CD9 promoted its transcription (Fig. 2A, left column). To test the calretinin induction is specifically related to CD9, multiple CD9 transfectants and cells transfected with another tetraspanin NAG-2 were examined. As shown in Fig. 2A, right column,

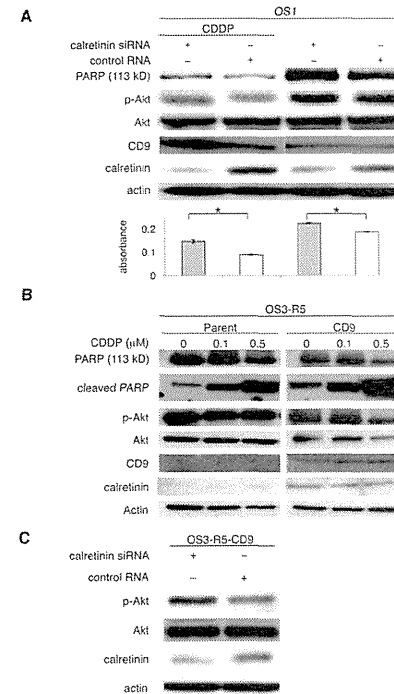


**Fig. 4.** Calretinin promotes apoptosis of CD9 (+) SCLC cells. (A) CD9 (+)/calretinin (+) OS1 cells were transfected with siRNAs against calretinin or control RNAs and cultured in low-serum conditions in the absence or presence of 5  $\mu$ M CDDP for 48 h. Cell lysates were analyzed for expressions of PARP (113 kD), phosphorylated Akt (p-Akt), total Akt, CD9, and calretinin by immunoblotting. Anti- $\beta$ -actin blots were used as the internal control (upper). Viable cells were quantified with a cell counting kit (lower).  $^*P < 0.01$ . (B) The parent and CD9 transfected of OS3-R5 were cultured in low-serum conditions in the indicated concentrations of CDDP for 48 h. Cell lysates were analyzed for expressions of PARP (113 kD), cleaved PARP, phosphorylated Akt, total Akt, CD9, and calretinin by immunoblotting. (C) OS3-R5-CD9 cells were transfected with siRNAs against calretinin or control RNAs and cultured in low-serum conditions for 48 h. Cell lysates were analyzed for expressions of phosphorylated Akt, total Akt, and calretinin by immunoblotting.

calretinin was almost absent in the parent, mock transfected, and NAG-2 transfected in immunoblotting, whereas calretinin was obviously present in three independent CD9 transfectants and its level was parallel to that of CD9. We further examined if CD9 and calretinin are co-expressed in a panel of lung tumor cell line (Fig. 2B). Consistent with our previous report that most SCLC cells lack CD9 [8], five of eight SCLC lines revealed no transcription and one cell line (OS2-RA) showed only marginal transcription of CD9 gene. The other two lines (OS1 and NCI-H209) clearly expressed CD9, and these CD9 (+) lines also expressed calretinin. Meanwhile, all three NSCLC lines were CD9 (+), but none of them expressed calretinin (Fig. 2B).

CD9 was next deleted by knockdown with siRNA in the SCLC line OS1, which expresses endogenous CD9. As shown in Fig. 2C, left column, the knockdown of CD9 suppressed the level of calretinin. In an

additional experiment, we have studied CD9 and calretinin expressions in multiple pleural mesothelioma cell lines and found that only NCI-H226 expresses both CD9 and calretinin in immunoblotting (Fig. S1). CD9 was knocked down in this mesothelioma line, but unlike OS1, the calretinin level was not affected (Fig. 2C, right column). Our recent report showed that endogenous CD9 is induced when the CD9 (-) SCLC line SBC-3 is exposed to an anticancer drug, cisplatin [10]. As shown in Fig. 2D, calretinin was co-induced with endogenous CD9 in the cisplatin-exposed SBC-3 cells.

We further investigated if CD9 is generally required for the expression of calretinin using tissues from wild-type and CD9 KO mice. Calretinin was expressed in liver and brain lysates of wild-type mice, and its levels were not affected by the loss of CD9, as evidenced by abundant expression of calretinin in the lysates from CD9 KO mice (Fig. S2). Together, regulation of calretinin expression by CD9 seemed to be specific to human SCLC cells.

### 3.3. CD9 is not physically associated with calretinin

To investigate co-expressions of CD9 and calretinin *in vivo*, a tissue microarray of SCLC was analyzed by immunohistochemistry. Among 30 patients, 11 were CD9 (+), 11 were calretinin (+), and 7 were double-positive, and association between CD9 expression and calretinin expression was weakly significant (Fig. 3A, table). Higher positive rate of CD9 (11/30) in SCLC tissues compared with that in SCLC cell lines [8] might be because some biopsy specimens were obtained from relapsed or metastatic lesions, which were more frequently CD9 (+) than pretreated primary tumors [10]. Representative staining of CD9 and calretinin in a double-positive specimen indicated that expression patterns of these proteins were different (Fig. 3A). CD9 was stained at the cell periphery, whereas calretinin showed nuclear and cytoplasmic staining (Fig. 3A, insets). Tetraspanins including CD9 are characterized by their propensity to form multiprotein complexes at the plasma membrane. To examine if calretinin is present in large protein complexes including CD9, co-precipitated proteins with CD9 was immunoblotted with anti-calretinin Ab. As shown in Fig. 3B, calretinin did not co-precipitate with CD9 in OS3-R5-CD9 cell lysate even using non-stringent detergent, Brij 99. Thus, calretinin was not present in the protein complex including CD9.

### 3.4. Calretinin promotes apoptosis of CD9 (+) SCLC cells

Our previous reports have shown that ectopic expression of CD9 increases apoptosis by attenuation of postadhesive phosphorylation of Akt [9] and that anticancer drugs induce endogenous CD9 in SCLC cell lines [10]. To examine the involvement of calretinin in apoptosis of SCLC cells, calretinin was knocked down with siRNA in CD9 (+)/calretinin (+) OS1 cells, and expression of PARP was examined as an indicator of apoptotic cell death [14]. Exposure of OS1 cells to 5  $\mu$ M cisplatin increased endogenous CD9 and calretinin and enhanced apoptosis as evidenced by decrease of 113-kD PARP and decreased phosphorylation of Akt (Fig. 4A, control RNA). Knockdown of calretinin prevented the OS1 apoptosis regardless of the exposure to cisplatin (Fig. 4A, calretinin siRNA). It appeared that the calretinin knockdown slightly upregulated CD9; this might reflect an unknown feedback mechanism. Proapoptotic role of calretinin was also studied in OS3-R5 cells. The exposure to CDDP for only 48 h did not induce endogenous CD9 and calretinin in this cell line and, when compared with the parent cells, OS3-R5-CD9 cells expressing calretinin revealed higher sensitivity to CDDP, as evidenced by enhanced PARP cleavage and decreased Akt phosphorylation (Fig. 4B). After the exposure to 1  $\mu$ M CDDP for 48 h, viable cells of OS3-R5 and OS3-R5-CD9 were 56.1  $\pm$  1.8% and 20.1  $\pm$  2.7%, respectively ( $P = 0.01$ ). As shown in Fig. 4C, the knockdown of calretinin in OS3-R5-CD9 increased phosphorylation of Akt. These results suggest that calretinin may be a downstream mediator of apoptosis in CD9 (+) SCLC cells.

#### 4. Discussion

Our previous studies have proposed that the absence of tetraspanin CD9 contributes to highly malignant phenotype of SCLC and that CD9 may be a pivotal regulator of SCLC cell survival [8–10]. In the present study using a proteomics-based approach, we identified calretinin as a possible mediator of CD9-induced apoptosis in SCLC. Calretinin was present in CD9 (+) SCLC cell lines but not in CD9 (–) SCLC lines and CD9 (+) NSCLC lines. Ectopic or CDDP-induced expression of CD9 upregulated calretinin in SCLC lines. Knockdown of CD9 conversely down-regulated calretinin in an SCLC line but not in a mesothelima cell line. Furthermore, knockdown of calretinin increased Akt phosphorylation and decreased apoptosis in CD9 (+)/calretinin (+) SCLC cell lines. Although statistical significance in the association of CD9 and calretinin expressions was weak ( $P = 0.047$ ) in SCLC tissues, we speculate that this might be due to elimination of apoptotic CD9 (+)/calretinin (+) tumor cells *in vivo*.

Calretinin is a member of the calcium-binding protein EF-hand family first identified in the retina. Calcium-binding proteins including calretinin are expressed in neuronal subpopulations of the nervous system. Calretinin is involved in cellular functions including intracellular calcium buffering, messenger targeting, and the modulation of neuronal excitability. Modulation of calcium signaling by calretinin is important for timing and plasticity of synaptic events in neuronal networks. Some studies have suggested neuroprotective role of calretinin against calcium-induced cytotoxicity, whereas others reported opposite effects [15,16]. Of note, a recent report using colorectal cancer cells indicated that calretinin is induced following treatment with oxaliplatin or 5-FU and positively regulates apoptotic signals via as yet unknown mechanisms [14]. In line with this report, the present study suggested that calretinin mediates proapoptotic signaling in SCLC cells and for the first time showed that CD9 positively regulates the expression of calretinin. It has been established that tetraspanins including CD9 work as organizer of multiprotein complexes at the membrane [4,5]. Although calretinin has been reported to concentrate beneath the plasma membrane during maturation in neurons [17], it did not co-precipitate with CD9 in OS3-R5-CD9 cells, suggesting the presence of other mediators linking CD9 to enhanced expression of calretinin.

In conclusion, by proteomics-based approach, we have proposed a novel proapoptotic pathway that links the metastatic suppressor CD9 to the neuronal calcium-binding protein, calretinin, in SCLC. Induction of CD9/calretinin may at least partially account for its high sensitivity to chemotherapy and might provide clues to new therapeutic approach to suppress early growth, metastasis, and recurrence of SCLC.

#### Acknowledgments

We thank Y. Habe for secretarial assistance. This work was supported in part by a Grant-in-Aid for Scientific Research from the

Ministry of Education, Culture, Sports, Science and Technology and a Health and Labour Sciences Research Grant from the Ministry of Health, Labour and Welfare, Japan.

#### Supplementary material

Supplementary material associated with this article can be found, in the online version, at doi:10.1016/j.fob.2013.04.005.

#### References

- [1] Stovold R, Blackhall F, Meredith S, Hou J, Dive C, White A. (2012) Biomarkers for small cell lung cancer: neuroendocrine, epithelial and circulating tumor cells. *Lung Cancer* 76, 263–268.
- [2] Califano R, Abidin A.Z., Peck R., Faviere-Finn C., Lorigan P. (2012) Management of small cell lung cancer: recent developments for optimal care. *Drugs* 72, 471–490.
- [3] Kitamura H., Yazawa T., Sato H., Okudela K., Shimoyamada H. (2009) Small cell lung cancer: significance of RB alterations and TTF-1 expression in its carcinogenesis, phenotype, and biology. *Endocr. Pathol.* 20, 101–107.
- [4] Charrin S., Le Naur F., Silvie O., Milhiet P.E., Boucheix C., Rubinstein E. (2009) Lateral organization of membrane proteins: tetraspanins spin their web. *Biochem. J.* 420, 133–154.
- [5] Yanez-Mo M., Barreiro O., Gordon-Alonso M., Sala-Valdes M., Sanchez-Madrid F. (2009) Tetraspanin-enriched microdomains: a functional unit in cell plasma membranes. *Trends Cell. Biol.* 19, 434–446.
- [6] Malik F.A., Sanders A.J., Jiang W.G. (2009) KAI-1/CD82, the molecule and clinical implication in cancer and cancer metastasis. *Histol. Histopathol.* 24, 519–530.
- [7] Wang H.X., Li Q., Sharma C., Knoblich K., Hemler M.E. (2011) Tetraspanin protein contributions to cancer. *Biochem. Soc. Trans.* 39, 547–552.
- [8] Funakoshi T., Tachibana I., Hoshida Y., Kimura H., Takeda Y., Kijima T. et al. (2003) Expression of tetraspanins in human lung cancer cells: frequent downregulation of CD9 and its contribution to cell motility in small cell lung cancer. *Oncogene* 22, 674–687.
- [9] Saito Y., Tachibana I., Takeda Y., Yamane H., He P., Suzuki M. et al. (2006) Absence of CD9 enhances adhesion-dependent morphologic differentiation, survival, and matrix metalloproteinase-2 production in small cell lung cancer cells. *Cancer Res.* 66, 9557–9565.
- [10] Kohno S., Kijima T., Otani Y., Mori M., Minami T., Takahashi R. et al. (2010) Cell surface tetraspanin CD9 mediates chemoresistance in small cell lung cancer. *Cancer Res.* 70, 8025–8035.
- [11] Kumagai T., Taniie Y., Osaki T., Hosoe S., Tachibana I., Ueno K. et al. (1996) Eradication of Myc-overexpressing small cell lung cancer cells transfected with herpes simplex virus thymidine kinase gene containing Myc-Max response elements. *Cancer Res.* 56, 354–358.
- [12] Shevchenko A., Wilm M., Vorm O., Mann M. (1996) Mass spectrometric sequencing of proteins silver-stained polyacrylamide gels. *Anal. Chem.* 68, 850–858.
- [13] Yamane H., Tachibana I., Takeda Y., Saito Y., Tamura Y., He P. et al. (2005) Propionibacterium acnes-induced hepatic granuloma formation is impaired in mice lacking tetraspanin CD9. *J. Pathol.* 205, 486–492.
- [14] Boyer J., Allen W.L., McLean E.C., Wilson P.M., McCulla A., Moore S. et al. (2006) Pharmacogenomic identification of novel determinants of response to chemotherapy in colon cancer. *Cancer Res.* 66, 2765–2777.
- [15] Camp A.J., Wijesinghe R. (2009) Calretinin: modulator of neuronal excitability. *Int. J. Biochem. Cell Biol.* 41, 2118–2121.
- [16] Barinka F., Druga R. (2010) Calretinin expression in the mammalian neocortex: a review. *Physiol. Res.* 59, 665–677.
- [17] Hack N.J., Wride M.C., Charters K.M., Kater S.B., Parks T.N. (2000) Developmental changes in the subcellular localization of calretinin. *J. Neurosci.* 20, RC67.

Your article 11-0810.R1 (22993) from *Inflammatory Bowel Diseases* is available for download  
*Inflammatory Bowel Diseases* © Published by John Wiley & Sons, Inc.

Dear Author,

Your article page proofs for IBD are ready for review. John Wiley & Sons has made this article available to you online for faster, more efficient editing. Please follow the instructions below and you will be able to access a PDF version of your article as well as relevant accompanying paperwork.

YOUR PAGE PROOFS ARE AVAILABLE IN PDF FORMAT; please refer to this URL address

<http://115.111.50.156/jw/retrieval.aspx?pwd=a0fc21b57564>

Login: your e-mail address; Password: a0fc21b57564

The site contains 1 file. You will need to have Adobe Acrobat Reader software to read these files. This is free software and is available for user downloading at <http://www.adobe.com/products/acrobat/readstep.html>.

This file contains:

Reprint Order Information and A copy of your page proofs for your article

After reading the PDF file, please check the page proofs carefully and:

- 1) indicate changes or corrections in the margin of the page proofs; either electronically or by hand (which should then be scanned/emailed back).
- 2) answer all queries (footnotes A,B,C, etc.) on the last page of the PDF proof;
- 3) proofread any tables and equations carefully;
- 4) check that any Greek, especially "mu", has translated correctly.

Within 48 hours, please return the following via email: Original PDF set of page proofs, (NOTE: articles cannot print without the category number and signed copyright form)

If you experience technical problems accessing your proof, please contact [wileycs@kwglobal.com](mailto:wileycs@kwglobal.com). Be sure to include your article number(11-0810.R1).

This e-proof is to be used only for the purpose of returning corrections to the publisher.

Sincerely,

Jessica Rodwick,

Associate Production Manager | Journal Content Management

Wiley Blackwell | John Wiley & Sons, Inc.

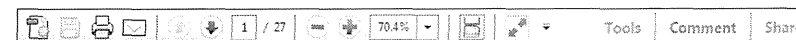
Phone: 201-748-6670; E-mail: [ibdprod@wiley.com](mailto:ibdprod@wiley.com)

Refer to journal acronym and article production number (i.e., IBD 0000 for *Inflammatory*)

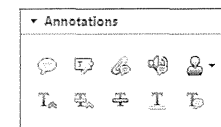
USING e-ANNOTATION TOOLS FOR ELECTRONIC PROOF CORRECTION

Required software to e-annotate PDFs: **Adobe Acrobat Professional** or **Adobe Reader** (version 8.0 or above). (Note that this document uses screenshots from **Adobe Reader X**)  
 The latest version of Acrobat Reader can be downloaded for free at: <http://get.adobe.com/reader/>

Once you have Acrobat Reader open on your computer, click on the Comment tab at the right of the toolbar:



This will open up a panel down the right side of the document. The majority of tools you will use for annotating your proof will be in the Annotations section, pictured opposite. We've picked out some of these tools below:



111 RIVER STREET, HOBOKEN, NJ 07030

**\*\*\*IMMEDIATE RESPONSE REQUIRED\*\*\***

Your article will be published online via Wiley's EarlyView® service ([wileyonlinelibrary.com](http://wileyonlinelibrary.com)) shortly after receipt of corrections. EarlyView® is Wiley's online publication of individual articles in full text HTML and/or pdf format before release of the compiled print issue of the journal. Articles posted online in EarlyView® are peer-reviewed, copyedited, author corrected, and fully citable via the article DOI (for further information, visit [www.doi.org](http://www.doi.org)). EarlyView® means you benefit from the best of two worlds--fast online availability as well as traditional, issue-based archiving.

Please follow these instructions to avoid delay of publication.

**READ PROOFS CAREFULLY**

- This will be your only chance to review these proofs. **Please note that once your corrected article is posted online, it is considered legally published, and cannot be removed from the Web site for further corrections.**
- Please note that the volume and page numbers shown on the proofs are for position only.

**ANSWER ALL QUERIES ON PROOFS** (Queries for you to answer are attached as the last page of your proof.)

- Mark all corrections directly on the proofs. Note that excessive author alterations may ultimately result in delay of publication and extra costs may be charged to you.

**CHECK FIGURES AND TABLES CAREFULLY**

- Check size, numbering, and orientation of figures.
- All images in the PDF are downsampled (reduced to lower resolution and file size) to facilitate Internet delivery. These images will appear at higher resolution and sharpness in the printed article.
- Review figure legends to ensure that they are complete.
- Check all tables. Review layout, title, and footnotes.

RETURN  **PROOFS**

**CTA (If you have not already signed one)**

**RETURN IMMEDIATELY AS YOUR ARTICLE WILL BE POSTED ONLINE SHORTLY AFTER RECEIPT; EMAIL PROOFS TO:**

**QUESTIONS?**

Jessica Rodwick, Associate Production Manager  
 Phone: 201-748-6670  
 E-mail: [ibdprod@wiley.com](mailto:ibdprod@wiley.com)  
 Refer to journal acronym and article production number (i.e., IBD 0000 for Inflammatory

— 144 —

**1. Replace (Ins) Tool – for replacing text.**

Strikes a line through text and opens up a text box where replacement text can be entered.

**How to use it**

- Highlight a word or sentence.
- Click on the Replace (Ins) icon in the Annotations section.
- Type the replacement text into the blue box that appears.

**2. Strikethrough (Del) Tool – for deleting text.**

Strikes a red line through text that is to be deleted.

**How to use it**

- Highlight a word or sentence.
- Click on the Strikethrough (Del) icon in the Annotations section.

**3. Add note to text Tool – for highlighting a section to be changed to bold or italic.**

Highlights text in yellow and opens up a text box where comments can be entered.

**How to use it**

- Highlight the relevant section of text.
- Click on the Add note to text icon in the Annotations section.
- Type instruction on what should be changed regarding the text into the yellow box that appears.

**4. Add sticky note Tool – for making notes at specific points in the text.**

Marks a point in the proof where a comment needs to be highlighted.

**How to use it**

- Click on the Add sticky note icon in the Annotations section.
- Click at the point in the proof where the comment should be inserted.
- Type the comment into the yellow box that appears.

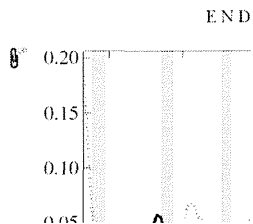
USING e-ANNOTATION TOOLS FOR ELECTRONIC PROOF CORRECTION

5. Attach File Tool – for inserting large amounts of text or replacement figures.

Inserts an icon linking to the attached file in the appropriate place in the text.

How to use it

- Click on the Attach File icon in the Annotations section.
- Click on the proof to where you'd like the attached file to be linked.
- Select the file to be attached from your computer or network.
- Select the colour and type of icon that will appear in the proof. Click OK.



6. Add stamp Tool – for approving a proof if no corrections are required.

Inserts a selected stamp onto an appropriate place in the proof.

How to use it

- Click on the Add stamp icon in the Annotations section.
- Select the stamp you want to use. (The Approved stamp is usually available directly in the menu that appears).
- Click on the proof where you'd like the stamp to appear. (Where a proof is to be approved as it is, this would normally be on the first page).

of the business cycle, starting with the on perfect competition, constant ret...  
 APPROVED  
 otaki (1987). has introduced produc general equilibrium models with nomin...

Drawing Markups

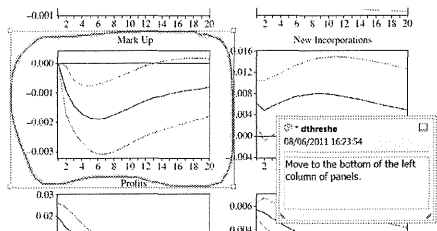


7. Drawing Markups Tools – for drawing shapes, lines and freeform annotations on proofs and commenting on these marks.

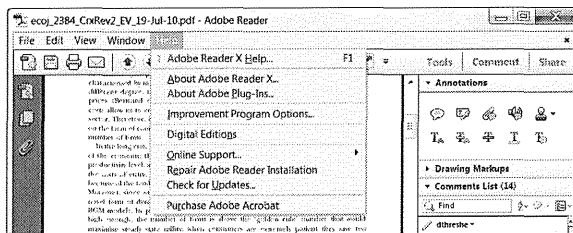
Allows shapes, lines and freeform annotations to be drawn on proofs and for comment to be made on these marks..

How to use it

- Click on one of the shapes in the Drawing Markups section.
- Click on the proof at the relevant point and draw the selected shape with the cursor.
- To add a comment to the drawn shape, move the cursor over the shape until an arrowhead appears.
- Double click on the shape and type any text in the red box that appears.



For further information on how to annotate proofs, click on the Help menu to reveal a list of further options:



Additional reprint purchases

Should you wish to purchase additional copies of your article, please click on the link and follow the instructions provided:

<https://caesar.sheridan.com/reprints/rcdir.php?pub=10089&acro=IBD>

Corresponding authors are invited to inform their co-authors of the reprint options available.

Please note that regardless of the form in which they are acquired, reprints should not be resold, nor further disseminated in electronic form, nor deployed in part or in whole in any marketing, promotional or educational contexts without authorization from Wiley. Permissions requests should be directed to mail to: [permissionsus@wiley.com](mailto:permissionsus@wiley.com)

For information about 'Pay-Per-View and Article Select' click on the following link: [wileyonlinelibrary.com/aboutus/ppv-articleselect.html](http://wileyonlinelibrary.com/aboutus/ppv-articleselect.html)

**COLOR REPRODUCTION IN YOUR ARTICLE**

Color figures were included with the final manuscript files that we received for your article. Because of the high cost of color printing, we can only print figures in color if authors cover the expense.

Please indicate if you would like your figures to be printed in color or black and white. Color images will be reproduced online in *Wiley Online Library* at no charge, whether or not you opt for color printing.

**Failure to return this form will result in the publication of your figures in black and white.**

JOURNAL Inflammatory Bowel Diseases VOLUME \_\_\_\_\_ ISSUE \_\_\_\_\_

TITLE OF MANUSCRIPT \_\_\_\_\_

MS. NO. \_\_\_\_\_ NO. OF COLOR PAGES \_\_\_\_\_ AUTHOR(S) \_\_\_\_\_

No. Color Pages	Color Charges	No. Color Pages	Color Charges	No. Color Pages	Color Charges
1	500	5	2500	9	4500
2	1000	6	3000	10	5000
3	1500	7	3500	11	5500
4	2000	8	4000	12	6000

\*\*\*Please contact the Production Editor for a quote if you have more than 12 pages of color\*\*\*

Please print my figures in black and white

Please print my figures in color

**BILL TO:**

Name \_\_\_\_\_ Purchase Order No. \_\_\_\_\_

Institution \_\_\_\_\_ Phone \_\_\_\_\_

Address \_\_\_\_\_ Fax \_\_\_\_\_

\_\_\_\_\_ E-mail \_\_\_\_\_

— 146 —

ORIGINAL ARTICLE

**Lectin-based Immunoassay for Aberrant IgG Glycosylation as the Biomarker for Crohn's Disease**

Shinichiro Shinzaki, MD, PhD,<sup>\*,†</sup> Eri Kuroki, MSc,<sup>\*</sup> Hideki Iijima, MD, PhD,<sup>†</sup> Norika Tatsunaka, MSc,<sup>\*</sup> Mayuko Ishii, BSc,<sup>\*</sup> Hironobu Fujii, BSc,<sup>\*</sup> Yoshihiro Kamada, MD, PhD,<sup>\*,†</sup> Taku Kobayashi, MD, PhD,<sup>†</sup> Narihiro Shibukawa, MD,<sup>†</sup> Takahiro Inoue, MD,<sup>†</sup> Masahiko Tsujii, MD, PhD,<sup>†</sup> Shunsaku Takeishi, PhD,<sup>§</sup> Tsunekazu Mizushima, MD, PhD,<sup>||</sup> Atsushi Ogata, MD, PhD,<sup>§</sup> Tetsuji Naka, MD, PhD,<sup>\*\*\*</sup> Scott E. Plevy, MD,<sup>†</sup> Tetsuo Takehara, MD, PhD,<sup>†</sup> and Eiji Miyoshi, MD, PhD<sup>\*</sup>

**Background:** Easily measured and clinically useful biomarkers for inflammatory bowel disease (IBD) are required to advance patient care. We previously reported that the agalactosyl fraction among fucosylated IgG oligosaccharides is increased in IBD, especially Crohn's disease (CD). The present study aimed to establish a simple detection system for aberrant glycosylated IgG based on lectin-oligosaccharide interactions.

**Methods:** Lectins with higher affinity to serum IgG from IBD patients than healthy volunteers (HV) were screened by lectin microarray. Binding of selected lectins to agalactosyl IgG was definitively confirmed using step-by-step glycosidase treatment. Using the selected lectins, a lectin-enzyme-linked immunosorbent assay system was established and its clinical utility was investigated in a total of 410 (249 Japanese and 161 American) IBD patients, disease controls, and HVs.

**Results:** *Agaricus bisporus* Agglutinin (ABA) and *Griffonia simplicifolia* Lectin-II(GSL-II) had higher affinity for serum agalactosyl IgG from IBD patients, especially those with CD, compared to HV. Agalactosyl IgG levels measured by a lectin-enzyme immunoassay (EIA) with ABA or GSL-II were significantly increased in CD compared with HV and disease controls. Agalactosyl IgG levels significantly correlated with disease activity, showed higher predictability of therapeutic outcomes for CD than C-reactive protein levels, and exhibited higher specificity for diagnosing IBD in combination with anti-*Saccharomyces cerevisiae* antibody (ASCA). Validation analysis showed that agalactosyl IgG levels were significantly increased in Japanese and American CD patients.

**Conclusions:** A lectin-EIA for agalactosyl IgG is a novel biomarker for IBD, especially in patients with CD.

(*Inflamm Bowel Dis* 2012;000:000-000)

**Key Words:** inflammatory bowel disease, Crohn's disease, biomarker, oligosaccharides, IgG

Additional Supporting Information may be found in the online version of this article.

Received for publication March 23, 2012; Accepted March 26, 2012.  
From the <sup>\*</sup>Department of Molecular Biochemistry and Clinical Investigation, Osaka University Graduate School of Medicine, Suita, Osaka, Japan, <sup>†</sup>Department of Gastroenterology and Hepatology, Osaka University Graduate School of Medicine, Suita, Osaka, Japan, <sup>‡</sup>Center for Gastrointestinal Biology and Diseases, University of North Carolina School of Medicine, Chapel Hill, North Carolina, USA, <sup>§</sup>DGP BioScience Ltd., Sapporo, Hokkaido, Japan, <sup>||</sup>Department of Surgery, Osaka University Graduate School of Medicine, Suita, Osaka, Japan, <sup>¶</sup>Department of Respiratory Medicine, Allergy and Rheumatic Diseases, Osaka University Graduate School of Medicine, Suita, Osaka, Japan, <sup>\*\*</sup>Laboratory for Immune Signal, National Institute of Biomedical Innovation, Ibaraki, Osaka, Japan.

The first two authors contributed equally to this work.  
Reprints: Eiji Miyoshi, MD, PhD, Department of Molecular Biochemistry and Clinical Investigation, Osaka University Graduate School of Medicine, 1-7 Yamadaoka, Suita, Osaka 565-0871, Japan (e-mail: emiyoshi@sahs.med.osaka-u.ac.jp).

Copyright © 2012 Crohn's & Colitis Foundation of America, Inc.  
DOI 10.1002/ibd.22993  
Published online 00 Month 2012 in Wiley Online Library (wileyonlinelibrary.com).

The human inflammatory bowel diseases (IBD), Crohn's disease (CD) and ulcerative colitis (UC), are characterized by chronic relapsing and remitting inflammation in the digestive tract. Although genetic predisposition, environmental factors, and altered immune responses have pivotal roles in the pathogenesis of IBD, precise etiologies remain unknown. Despite recent therapeutic advances,<sup>1,2</sup> surgical care remains a mainstay of IBD.<sup>3</sup> Therefore, a biomarker that reflects clinical course and therapeutic outcome is in high demand. Several serologic markers have been developed for the diagnosis of IBD such as anti-*Saccharomyces cerevisiae* antibody (ASCA),<sup>4</sup> peripheral antineutrophil cytoplasmic antibody,<sup>5</sup> or anti-outer membrane porin protein C, and anti-CBir1 flagellin.<sup>6</sup> However, these antibodies generally lack diagnostic and prognostic sensitivity and specificity to alter clinical decision making.

Immunoglobulin (Ig) G carries N-linked oligosaccharides at the Cgamma2 domain of the Fc fragment at asparagine 297, all of which are biantennary complex-type with or without bisecting N-acetylglucosamine (GlcNAc), core-

TABLE 1. Patient Characteristics: Japanese Population

	CD (N = 82)	UC (N = 70)	HV (N = 78)	DC (N = 19)	SLE (N = 29)	RA (N = 20)
Male/Female	22/60	31/39	39/39	9/10	5/24	2/18
Age, yr, mean (SD)	38 (11)	39 (14)	45 (11)	35 (16)	33 (14)	52 (16)
Age at diagnosis, yr, mean (SD)	28 (10)	33 (13)				
Disease location, N						
Small bowel/colon/both/unknown	27/11/42/2					
Extensive/left colon/rectum/unknown		28/26/14/2				
Treatment, N (%)						
Salazosulfapyridine or mesalazine	72 (88)	59 (84)				
Steroids	4 (5)	9 (13)				
Immunomodulators	10 (12)	2 (3)				
Anti-TNF-alpha antibodies	7 (9)	0 (0)				
CRP, mg/dL, mean (SD)	1.0 (1.6)	0.4 (1.1)				
CDAI (CD) or CAI (UC), mean (SD)	153 (92)	3.3 (4.0)				

fuco-6, galactose, and sialic acid residues. Our previous analysis of IgG oligosaccharides revealed that the agalactosyl fraction among fucosylated oligosaccharides was significantly higher in patients with CD and UC than in healthy volunteers (HV) and disease controls (DC). Fucosylated agalactosyl IgG levels closely correlated with disease activity and clinical course in IBD patients, and had a significantly higher sensitivity to diagnose IBD compared with ASCA.<sup>7</sup> We also reported that agalactosyl IgG oligosaccharides enhanced antibody-dependent phagocytosis, suggesting that oligosaccharide alterations of IgG are not only a marker of IBD but also functionally modulate immune function.<sup>8</sup> The current analytic methodology, however, requires researchers to perform multistep complicated procedures to acquire an IgG oligosaccharide chart using high-performance liquid chromatography (HPLC), so the development of an easier detection system is necessary for widespread clinical application.

There have been technical obstacles in establishing simple detection systems for oligosaccharides due to difficulties in purifying an oligosaccharide-specific antibody. Although several oligosaccharide structures can be measured by lectin-antibody enzyme immunoassay (EIA),<sup>9</sup> lectins have a lower affinity and specificity for oligosaccharides than specific antibodies.<sup>10</sup> To overcome these problems, in the present study we developed a lectin-EIA system by using multiple lectins to detect agalactosyl IgG as a new serologic marker for IBD.

MATERIALS AND METHODS

Subjects

Serum samples were collected from 82 patients with CD, 70 patients with UC, 72 age/gender-matched unrelated HVs, and

19 patients with colonic inflammation including appendicitis, diverticulitis, and ischemic colitis (DCs). These participants were Japanese recruited at the Department of Gastroenterology and Hepatology, Osaka University Hospital (Suita, Osaka, Japan), the Department of Gastroenterology, Osaka Rosai Hospital (Sakai, Osaka, Japan). Serum samples of patients with systemic lupus erythematosus (SLE) and rheumatoid arthritis (RA) were provided by the Department of Respiratory Medicine, Allergy and Rheumatic Diseases, Osaka University Hospital. Patient characteristics are presented in Table 1. On the validation analysis, American serum samples were collected from 103 patients with CD, 39 patients with UC, and 19 HVs, who were recruited at the Department of Medicine, University of North Carolina Hospital (Chapel Hill, NC). Patient characteristics are presented in Table 2. The Ethics Committee at each hospital approved the study protocol and written informed consent was obtained from each participant. Patients were diagnosed with CD or UC according to endoscopic, radiologic, histologic, and clinical criteria.<sup>11-13</sup> Patients with CD were classified by age at diagnosis (A1, below 16 years old; A2, between 17 and 40 years old; A3, above 40 years old), location (L1, ileal; L2, colonic; L3, ileocolonic; L4, isolated upper disease), and behavior (B1, nonstricturing and nonpenetrating; B2, stricturing; B3, penetrating) according to the Montreal Classification.<sup>14</sup> Clinical activities were determined using the Crohn's Disease Activity Index (CDAI) for CD<sup>15</sup> or the Clinical Activity Index (CAI) for UC.<sup>16</sup> Infliximab maintenance therapy<sup>17</sup> was performed on biologic therapy-naïve CD patients. Clinical responders by infliximab therapy were defined as the patients whose CDAI scores at week 30 were less than 150 or decreased more than 70 from the pretreatment scores.

IgG Oligosaccharide Analysis by HPLC

Serum IgG oligosaccharide analysis was performed as described previously.<sup>7</sup> Briefly, IgG was purified using Protein

TABLE 2. Patient Characteristics: U.S. Population

	CD (N = 103)	UC (N = 39)	HV (N = 19)
Male/Female	49/54	23/16	11/8
Age, yr, mean (SD)	39 (14)	43 (18)	31 (4)
Age at diagnosis, yr, mean (SD)	27 (9)	33 (7)	
Duration of disease, yr, mean (SD)	12 (9)	10 (7)	
Disease location (N)			
Small bowel/colon/both/others	28/24/49/3		
Extensive/left colon/rectum/unknown		24/11/3/1	
Treatment, N (%)			
Salazosulfapyridine or mesalazine	25 (24)	20 (51)	
Steroids	15 (14)	9 (23)	
Immunomodulators	35 (34)	4 (10)	
Anti-TNF-alpha biologics	23 (22)	11 (28)	

G sepharose (Amersham Pharmacia Biotech, Buckinghamshire, UK). N-linked oligosaccharides were released from serum IgG by Glycopeptidase F (Takara Bio, Shiga, Japan) and labeled with 2-aminopyridine by GlycoTag (Takara Bio). Pyridylamino- (PA-) oligosaccharides from IgG were analyzed on a reverse-phase HPLC system (Waters, Milford, MA).

Lectin Microarray

Total pattern of oligosaccharide structures in serum IgG was investigated with evanescent-field fluorescence-assisted lectin microarray.<sup>18</sup> Forty-five kinds of lectin were immobilized on the glass slide in triplicate and ≈250 ng/mL of IgG in phosphate-buffered saline (PBS) with 1% Triton X-100 was applied to the array. To label target glycoproteins, Cy3 mono-reactive dye (GE Healthcare Biosciences, Chalfont St Giles, UK) was used in this analysis. Detailed procedures were described previously.<sup>18</sup> Fluorescence intensity of all lectins and that of lower signal-lectins were analyzed independently.

Step-by-step Glycosidase Treatment Followed by Lectin Blotting

Purified serum IgG was obtained and incubated with sialidase, beta-galactosidase, and glucosaminidase by enzymatic carborelease kit (QA Bio, Palm Desert, CA), according to the manufacturer's instructions. Lectin blotting was performed in each step of glycosidase treatment.

Lectin Blotting

Eight micrograms of purified serum IgG was separated 10% sodium dodecyl sulfate-polyacrylamide gel electrophoresis (SDS-PAGE) under reducing conditions and then transferred to a nitrocellulose membrane (GE Healthcare Biosciences).

The membrane was incubated overnight at 4°C with 3% bovine serum albumin in Tris-buffered saline containing 0.05% Tween 20 (TBS-T), and then for 1 hour at room temperature with biotinylated *Agaricus bisporus* Agglutinin (ABA) (1 µg/mL, Seikagaku biobusiness, Tokyo, Japan), *Griffonia simplicifolia* Lectin-II (GSL-II) (2 µg/mL, Vector Laboratories, Burlingame, CA), *Concanavalin A* (ConA) (0.5 µg/mL, Seikagaku biobusiness), *Sambucus sieboldiana* Agglutinin (SSA) (1 µg/mL, Seikagaku biobusiness), or *Ricinus communis* Agglutinin I (RCA120) (1 µg/mL, Seikagaku biobusiness) in 3% bovine serum albumin in TBS-T. After washing with TBS-T three times, the membrane was incubated with Vectastain ABC kit (Vector Laboratories) for 20 minutes, then washed with TBS-T three times. Staining was performed with ECL reagent (GE Healthcare, Milwaukee, WI).

Lectin-EIA

Purified IgGs from sera of patients and HVs (adjusted to 5 µg/well) were prepared with sample diluents (PBS containing 0.1% bovine serum albumin [BSA] and 0.05% Tween 20) containing SDS (final concentration is 0.05%) for 1 hour. Flat-bottomed 96-well streptavidin-precoated microtiter plate (Nalge Nunc International, Tokyo, Japan) was coated with 50 µL/well of biotinylated ABA (0.33 µg/mL) and/or biotinylated GSL-II (0.67 µg/mL) with 0.05% BSA in PBS for 1 hour at room temperature. After washing the plate four times with PBS containing 0.05% Tween 20 (PBS-T), 50 µL/well of the prepared IgG was added. After incubation for 1 hour, the plate was washed four times with PBS-T, then 100 µL/well of 0.1% BSA in PBS was added to block nonspecific protein binding sites. After incubation for 1 hour, the plate was washed four times with PBS-T, then 50 µL/well of a 1/2000-diluted solution of alkaline phosphatase-conjugated antibody against human IgG (SouthernBiotech, Birmingham, AL) was added. After incubation for 1 hour, the plate was washed four times with PBS-T and added 50 µL/well of 0.1M glycine buffer (pH 10.4) with phosphate substrate (Sigma-Aldrich, St. Louis, MO), and then incubated for 20 minutes. The optical density (OD) was measured at 405 nm. All experiments were run in duplicate and the median was used as the final value for each sample. Agalactosyl IgG standard was kindly provided by Sanko Junyaku (Tokyo, Japan).<sup>19</sup>

Statistical Analyses

Differences between measurements and groups were tested with Mann-Whitney U-test. A P value less than 0.05 was considered statistically significant. A receiver operated characteristic (ROC) curve was generated by plotting sensitivity versus 1 - specificity for every possible cutoff score<sup>20,21</sup> and area under the ROC curve was calculated. The optimal cutoff scores were determined by ROC curve, and then sensitivities, specificities, positive predictive values (PPV), and negative predictive values (NPV) were measured.

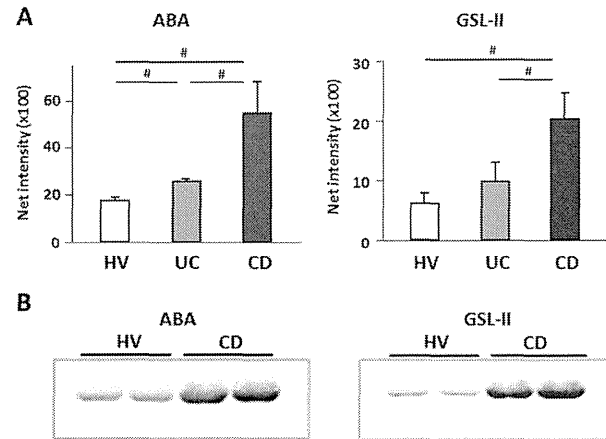


FIGURE 1. Binding levels of ABA and GSL-II to IgG *N*-linked oligosaccharides are higher in patients with IBD than in HVs. (A) Lectin microarray for serum IgGs from HV, patients with UC, and those with CD (five cases each). Among 45 lectins on the lectin microarray, results for ABA and GSL-II are shown. #*P* < 0.05. (B) Lectin blotting for serum IgGs from HV and CD (two cases each). Each blot is representative of three independent experiments with similar results.

All analyses were performed using JMP v. 8 software for Windows (SAS, Cary, NC).

**RESULTS**

**Lectin Microarray Analysis for Serum IgG Oligosaccharides**

To identify the most relevant lectin(s) characteristic for detecting agalactosyl IgG in IBD, we first screened serum by lectin microarray. Serum IgGs from patients with CD, UC, and HV were purified by protein G column liquid chromatography and a lectin-microarray was performed for each sample (Supporting Fig. 1). Among 45 lectins, only two lectins had higher affinity for IBD and potentially recognize *N*-linked agalactosyl oligosaccharides. Lectin microarray showed that the signal intensities of the lectins, ABA and GSL-II, were significantly higher in IBD patients, especially those with CD, than in HV (Fig. 1A). Lectin blot analysis, performed to confirm the results obtained from lectin-microarray, clearly showed that serum IgGs from CD patients had higher affinity for both ABA and GSL-II compared to those from HV (Fig. 1B).

**Both ABA and GSL-II Recognize ‘Agalactosyl IgG’**

Previous reports showed that both ABA and GSL-II recognize agalactosyl *N*-linked oligosaccharides.<sup>22,23</sup> These

studies were performed with frontal affinity chromatography using fluorescence-labeled oligosaccharides that are not attached to proteins. To confirm that both lectins recognize agalactosyl oligosaccharides attached to IgG, namely, “agalactosyl IgG,” we first investigated whether IgG itself was recognized by these lectins using IgG treated with a set of glycopeptidases to detach oligosaccharides from IgG. Depletion of oligosaccharides was confirmed by Coomassie brilliant blue (CBB) staining, which showed a slight decrease in the molecular weight of IgG (Fig. 2A). Glycopeptidase-treated IgG showed decreased affinity for ConA, which recognizes most *N*-linked oligosaccharides except those with a bisecting GlcNAc structure,<sup>24</sup> as well as to both ABA and GSL-II (Fig. 2A). These results indicate that ABA and GSL-II accurately recognize oligosaccharides attached to IgG. Next, a step-by-step glycosidase treatment followed by lectin blotting was performed to determine the characteristic oligosaccharide structure. First, IgG was treated by sialyase, which detaches sialic acid from sugar chains. The removal of sialic acid was confirmed by sialic acid binding lectin, SSA. Binding of ABA and GSL-II to the IgG, however, was unchanged (Fig. 2B). Next, sialyase-treated IgG was incubated with the galactose remover beta-galactosidase. Affinities of ABA and GSL-II to IgG were increased after the removal of galactose, whereas the affinity of RCA120, an *N*-linked

F2

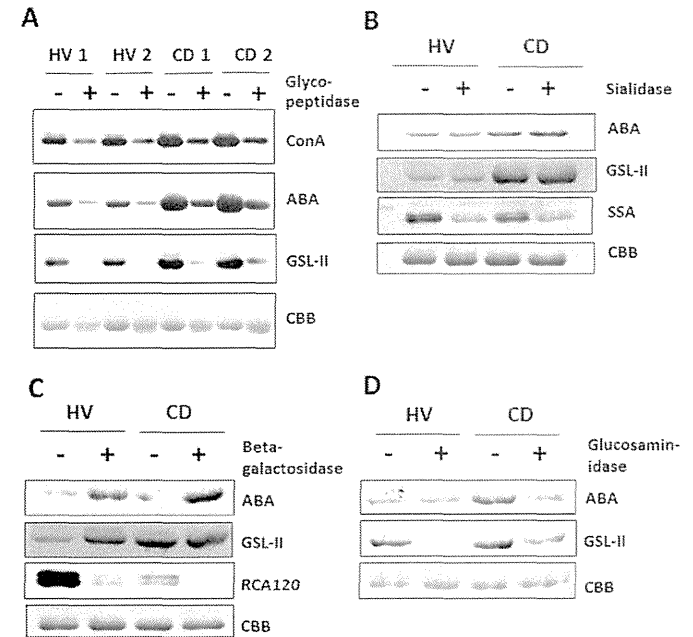


FIGURE 2. ABA and GSL-II recognize the *N*-linked oligosaccharide structure. (A) Purified serum IgGs from HV and CD (two cases each) were treated with glycopeptidase F to remove oligosaccharides from IgG. Binding of ABA, GSL-II, and ConA (binds *N*-linked oligosaccharides) to enzymatically treated or untreated IgGs was analyzed by lectin blotting. (B–D) Serum IgGs from HV and CD (two cases each) were treated with or without (B) sialidase, (C) beta-galactosidase, and (D) glucosaminidase in a step-by-step manner followed by lectin blotting. Each blot is representative of three independent experiments with similar results.

galactose binder, was decreased (Fig. 2C). Finally, galactosidase-treated IgG was incubated with glucosaminidase, which removes GlcNAc from mannose. Both ABA and GSL-II lectin blotting showed decreased binding affinities for IgG oligosaccharides (Fig. 2D). These findings indicate that both ABA and GSL-II recognize *N*-linked GlcNAc attached to IgG, namely “agalactosyl IgG.”

**Agalactosyl IgG Is Increased in IBD Patients by Lectin-EIA**

To quantify agalactosyl IgG by EIA, a standard curve using agalactosyl IgG was generated. First, oligosaccharide analysis of agalactosyl control IgG was performed by conventional HPLC methods.<sup>7</sup> The outer arm galactose was confirmed to be almost completely absent in control aga-

lactosyl IgG (Fig. 3A). Using this control IgG as an EIA standard, a lectin-EIA system for agalactosyl IgG (Agal-IgG) was developed by immobilizing both ABA and GSL-II on the same plate, by which an accurate standard curve with high *R*<sup>2</sup> ratio (0.9991) was generated (Fig. 3B). Using the standard curve, Agal-IgG levels were investigated in sera from human subjects. The levels of Agal-IgG in patients with CD were significantly increased than those with UC, HV, and DC, and the levels in patients with UC were also significantly higher than those with HV (Fig. 3C). Agal-IgG levels in patients with SLE or RA were also significantly higher than those with HV. Agal-IgG levels in patients with CD were significantly higher than those with SLE and relatively higher than those with RA. In addition, certain cases of CD showed dramatic increases in Agal-IgG

F3

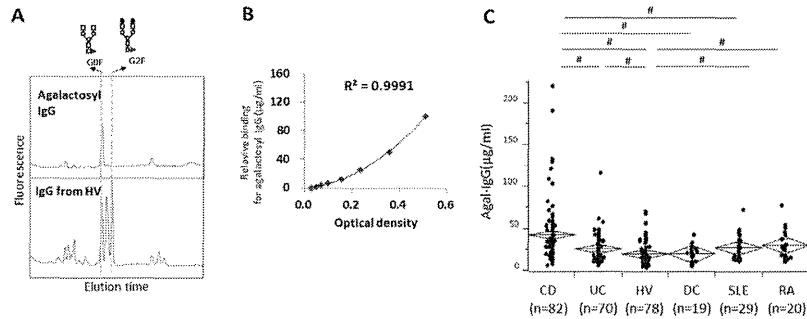


FIGURE 3. Agalactosyl IgG is increased in IBD patients by lectin-EIA. (A) Oligosaccharide structures from control agalactosyl IgG or serum IgG in HV were analyzed by HPLC. The outer arm galactose was almost completely absent in control agalactosyl IgG. This result is representative of three independent experiments. (B) To generate a standard curve, control agalactosyl IgG was diluted step-by-step and assayed for reactivity with ABA and GSL-II (Agal-IgG) by EIA. This result is representative of three independent experiments. (C) Agal-IgG levels of purified serum IgG from CD, UC, HV, DC, SLE, and RA by EIA. # $P < 0.05$ .

compared to other IBD and autoimmune diseases (Fig. 3C). These results indicate that Agal-IgG is increased in patients with IBD, especially with CD.

#### Agal-IgG Reflects Disease Activity and Clinical Course in CD

We next investigated whether values obtained by lectin-EIA (Agal-IgG) reflect disease classification, activity, and clinical course in IBD. Agal-IgG levels were significantly higher in CD patients whose onset age was below 16 (category A1) or between 17 and 40 (category A2) than in those above 40 (category A3) years of age at time of diagnosis (Fig. 4A). There were no significant age-related increases in Agal-IgG in either HV and CD patients (Supporting Fig. 2), suggesting that the influence of age-related change in agalactosyl IgG is very small because the participants are relatively young, and that the increase in Agal-IgG in CD patients is not related to aging but to younger onset of disease. There were no significant differences in the location (category L) or behavior (category B) of disease based on Agal-IgG levels (Fig. 4B,C). Agal-IgG levels were also not correlated with C-reactive protein (CRP) levels (data not shown). Moreover, Agal-IgG levels were significantly higher in patients with active CD (CDAI  $\geq 150$ ) than in patients in remission (CDAI  $< 150$ , Fig. 4D). When CD patients treated with infliximab scheduled maintenance therapy were divided into responders and nonresponders at 30 weeks after the initial infusion, the difference between Agal-IgG levels at week 6 and week 0 ( $\Delta$ Agal-IgG) was significantly higher in responders than in nonresponders (Fig. 4E), although the difference between CRP levels at

week 6 and week 0 ( $\Delta$ CRP) was unchanged in both groups (Fig. 4F). These results indicate that Agal-IgG could be a biomarker not only for detecting disease activity but also for predicting the clinical course of CD.

#### Combination of Agal-IgG and ASCA Increases Diagnostic Accuracy for CD

We then investigated the diagnostic accuracy of Agal-IgG for IBD by comparing with ASCA. We compared the sensitivity and specificity of Agal-IgG with those of ASCA for the discrimination of IBD by ROC curve and AUC analyses. The AUC was unchanged between Agal-IgG and ASCA for the differentiation of CD and HV (AUC of Agal-IgG vs. ASCA = 0.79 vs. 0.81; Fig. 5A), as well as CD and UC (AUC of Agal-IgG vs. ASCA = 0.69 vs. 0.72; Fig. 5B). The ROC curve, however, showed different patterns between Agal-IgG and ASCA; Agal-IgG had higher specificity than ASCA under high sensitivity conditions. There was no correlation between Agal-IgG and ASCA levels among all subjects (Fig. 5C). We then calculated the sensitivity and specificity of Agal-IgG/ASCA double-positive CD patients. By the ROC curve, the combination of Agal-IgG and ASCA positivity showed higher specificity than Agal-IgG or ASCA alone for the diagnosis of CD (Table 3).

#### Agal-IgG Levels Are Also Increased in American IBD Patients

To determine whether Agal-IgG levels are increased in a different geographic population, we investigated Agal-IgG levels in U.S. IBD patients and healthy volunteers.

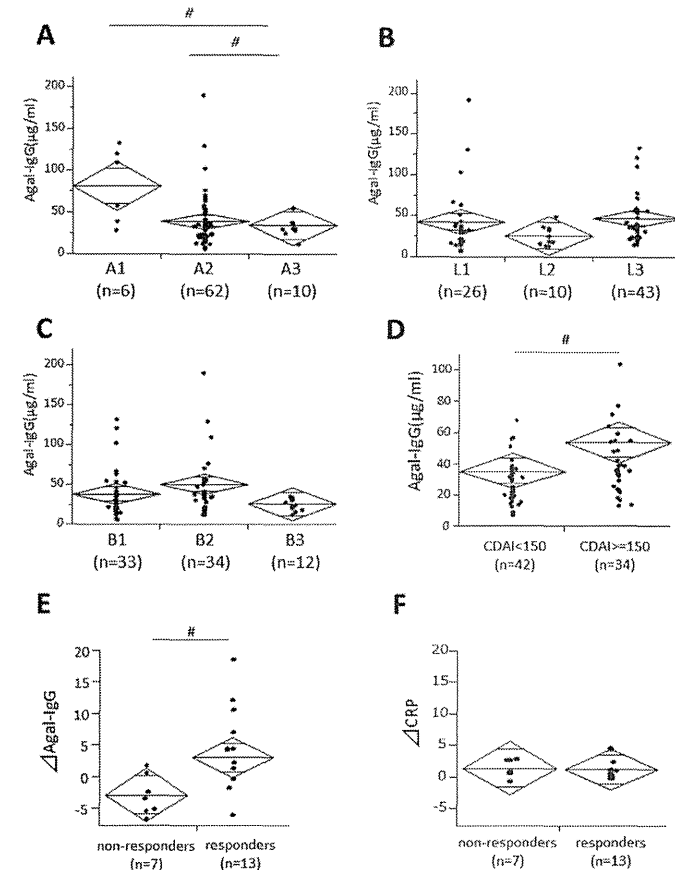


FIGURE 4. Agalactosyl IgG reflects disease activity and clinical course in CD. (A) Agal-IgG levels and age of disease onset (category A) in CD patients. Agal-IgG levels were significantly higher in patients with category A1 than A2 or A3. (B,C) Agal-IgG levels and disease location (category L, (B)) and disease behavior (category B, (C)) in CD patients. (D) Agal-IgG levels and disease activity in CD patients. Agal-IgG was higher in active patients (CDAI  $\geq 150$ ,  $n = 42$ ) than in patients in remission (CDAI  $< 150$ ,  $n = 34$ ). (E,F) Agal-IgG or CRP levels and clinical response to infliximab. Infliximab-naïve CD patients were treated with infliximab scheduled maintenance therapy. (E) The difference between Agal-IgG levels at week 6 and week 0 ( $\Delta$ Agal-IgG) was higher in responders than in nonresponders. (F) The difference between CRP levels at week 6 and week 0 ( $\Delta$ CRP) was unchanged in both groups.  $P < 0.05$ .

Agal-IgG levels were also significantly higher in IBD patients, especially in CD patients, than in healthy volunteers (Fig. 6A). In CD patients, Agal-IgG levels were significantly higher in patients with earlier onset category A1 or A2 than in those with category A3 (Fig. 6B). No significant differences were observed in category L or category B

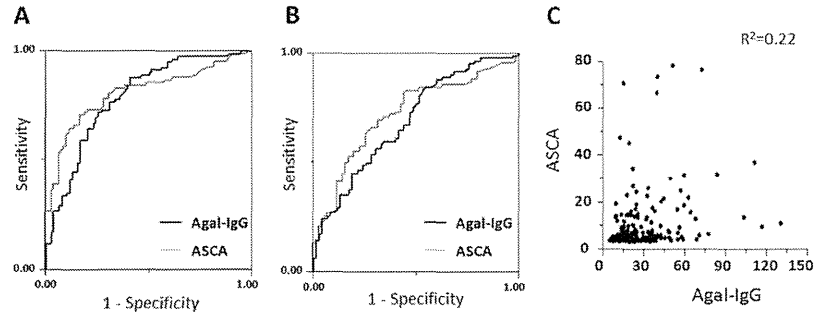


FIGURE 5. The combination of Agal-IgG and ASCA more efficiently differentiates CD. (A) The ROC curves for Agal-IgG and ASCA levels for discrimination between CD and HV, or (B) between CD and UC. (C) Correlation between Agal-IgG and ASCA levels in all subjects ( $n = 230$ ).

(Fig. 6C,D). These results were in excellent concordance with analyses for Japanese IBD patients (Figs. 3C, 4A–C), indicating Agal-IgG could be a biomarker for IBD patients irrespective of geography and consequently genetic background.

DISCUSSION

We previously reported that fucosylated agalactosyl IgG is increased in the sera of patients with IBD, and the extent of agalactosylation of fucosylated IgG is a potential diagnostic marker for IBD.<sup>7</sup> In the present study, we showed that both ABA and GSL-II preferentially recognize agalactosyl IgG, and affinities of both lectins to IgG were significantly increased in CD patients compared to HV. We also generated a lectin-EIA system in which an increase in agalactosyl IgG could be detected and determined that agalactosyl IgG is a useful diagnostic marker that reflects disease activity and clinical course of CD.

GSL-II binds to agalactosyl *N*-linked oligosaccharides with primary recognition of a GlcNAc residue and major

specificity for tri- or tetra-antennary structures.<sup>22</sup> ABA has been widely used to detect and capture *O*-linked oligosaccharides containing Galb1-3GalNAc.<sup>25,26</sup> However, ABA also has substantial affinity for mono-, bi-, and tri-antennary agalactosyl *N*-linked oligosaccharides.<sup>23</sup> Although these previous reports demonstrated affinity between lectin and agalactosyl *N*-linked oligosaccharides, the investigators used fluorescence-binding oligosaccharides as a substrate and did not confirm the affinity for glycoproteins, i.e., IgG. In the present study we therefore demonstrate for the first time that both ABA and GSL-II recognize native biantennary GlcNAc on *N*-linked IgG oligosaccharides without destroying the crystal structure of the IgG glycoprotein. Lectin microarray is a powerful tool for screening such types of lectins.

EIA is widely used as a simple system to quantify specific proteins; however, several problems make it difficult to apply the “protein-specific” EIA to an “oligosaccharide-specific” system. First, the lectin-oligosaccharide interaction is approximately one-tenth the affinity of antigen-

TABLE 3. Accuracy of Agal-IgG and ASCA to Differentiate (A) CD from HV, or (B) CD from UC

	Sensitivity	Specificity	PPV	NPV
(A)				
ASCA (+)	71% (58/82)	83% (65/78)	82% (58/71)	73% (65/89)
Agal-IgG (+)	88% (72/82)	59% (46/78)	69% (72/104)	82% (46/56)
ASCA (+)/Agal-IgG (+)	67% (55/82)	94% (72/78)	90% (55/61)	73% (72/99)
(B)				
ASCA (+)	70% (57/82)	69% (48/70)	72% (57/79)	66% (48/73)
Agal-IgG (+)	83% (68/82)	47% (33/70)	65% (68/105)	58% (33/57)
ASCA (+)/Agal-IgG (+)	62% (51/82)	84% (59/70)	82% (51/62)	66% (59/90)

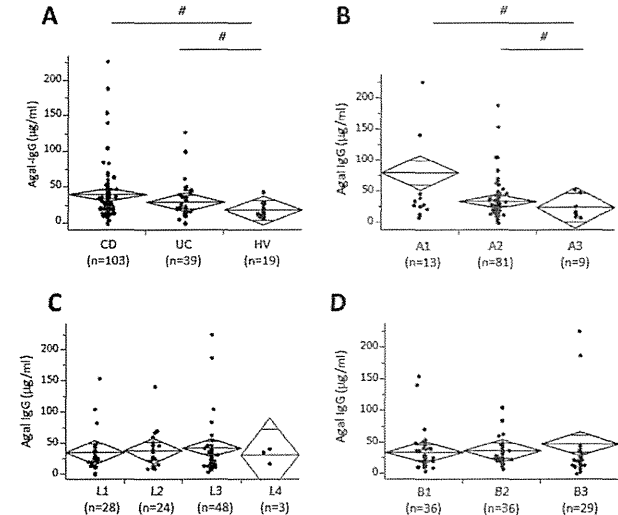


FIGURE 6. Agal-IgG levels are also increased in American IBD patients. (A) Agal-IgG levels of each purified serum IgG from CD, UC, and HV by EIA. (B) Agal-IgG levels and onset age (category A) in CD patients. Agal-IgG levels were significantly higher in patients with category A1 than with A2 or A3. (C,D) Agal-IgG levels and disease location (category L) (B) and behaviors (category B, C) in CD patients.

antibody binding,<sup>10</sup> so lectin-oligosaccharide complexes easily dissociate during the EIA procedure. Second, the recognition of an oligosaccharide by a lectin is not always specific for a single structure. Third, oligosaccharides are sometimes sterically encumbered by the surrounding protein so that lectins do not bind to glycoproteins compared to oligosaccharide structures without proteins. To overcome these problems, we adopted a simultaneous detection system by two lectins. We showed that both lectins recognize agalactosyl IgG oligosaccharides, but the binding affinity of each lectin to oligosaccharide might be subtly influenced by the surrounding protein structure.<sup>27</sup> The Agal-IgG EIA may have achieved a high sensitivity because each lectin contributes to bind to agalactosyl IgG. Another reason the dual lectin Agal-IgG EIA may be a sensitive and specific method is that nonspecific binding for each lectin may decrease due to the requirement for reduced concentrations: A higher concentration of a single lectin is necessary to generate a standard curve for agalactosyl IgG.

We previously reported on the significance of agalactosyl fraction of the fucosylated IgG oligosaccharides (G0F/G2F) in patients with IBD. It is interesting that fucosylated G0F/G2F is more specific than nonfucosylated aga-

lactosyl IgG in IBD.<sup>7</sup> Agal-IgG should be consistent with G0F/G2F by HPLC, because Agal-IgG theoretically indicates whole agalactosyl IgG, and because G0F/G2F is a major fraction of IgG oligosaccharides. In contrast, fucosylation of IgG alters biological activity of IgG including antibody-dependent cellular cytotoxicity, which might be due to conformation changes in the IgG Fc portion.<sup>28</sup> In our system ABA and GSL-II can recognize both the oligosaccharide structure and the 3D structure of the IgG Fc portion, whereas the HPLC system purely analyzes the oligosaccharide structure of IgG. The sensitivity and specificity of Agal-IgG for diagnosis of CD might, therefore, be slightly different from our previous study. However, Agal-IgG could be a marker for disease activity of CD and the combination of Agal-IgG and ASCA is a better marker for diagnosing IBD than ASCA alone, as discussed below. Furthermore, certain cases of CD showed dramatic increases in Agal-IgG measured by lectin-EIA, compared to other IBD and autoimmune diseases. Although we started the present study to establish more convenient methods to measure agalactosyl IgG levels than the HPLC system, Agal-IgG by lectin-EIA can possibly help elucidate the novel pathogenesis of CD. Further studies from both clinical and

basic approaches will be required for CD patients showing extremely high Agal-IgG levels.

Here we demonstrated that Agal-IgG is a useful diagnostic marker in combination with ASCA. ASCA is one of the most well-established serologic markers for diagnosing CD,<sup>4</sup> but ASCA alone does not possess enough power to diagnose CD with sufficient sensitivity or specificity. Therefore, ASCA has been combined with other markers, such as peripheral antineutrophil cytoplasmic antibody<sup>5</sup> or anti-outer membrane porin protein C, and anti-CBir1 flagellin.<sup>6</sup> In the present study, Agal-IgG itself showed almost the same sensitivity and specificity as ASCA for the discrimination of CD and HV or CD and UC; however, Agal-IgG was not strongly correlated with ASCA. The combination of Agal-IgG and ASCA could augment the specificity as a diagnostic marker partly because Agal-IgG might identify different subgroups of patients within CD than ASCA. Further investigation is necessary to assess whether the combination of Agal-IgG and ASCA is a better marker for diagnosing IBD than Agal-IgG or ASCA alone. Moreover, we showed that Agal-IgG may have higher predictability for response to infliximab compared with CRP (Fig. 4E,F). Agal-IgG can reflect different inflammatory conditions from CRP, because Agal-IgG is not increased in patients with acute intestinal inflammation (Fig. 3C), and because IgG has a long serum half-life of 3 weeks, whereas that of CRP is 4–6 hours. The decrease of Agal-IgG in 6 weeks of infliximab treatment may be, therefore, a novel marker for sustained response. If confirmed in larger prospective analyses, this finding could have important clinical implications.

In a validation study, we showed that Agal-IgG levels were also significantly increased in a non-Asian, U.S. cohort of IBD patients, especially in early onset (category A1/A2) CD patients. A previous report showed that disease location and clinical course are severer in patients whose onset is younger, and that the A3 group had a lower incidence of fistulas and fewer requirements for immunomodulators and corticosteroids.<sup>29</sup> Higher levels of Agal-IgG in category A1/A2 patients may therefore reflect disease severity in younger-onset patients. Although the mechanism has not been clarified, Agal-IgG can be useful especially for screening pediatric patients for whom invasive studies are hard to perform. Although clinical manifestations appear to be similar in all geographies, ethnic differences in genetic associations have been reported. For instance, mutations in the leucine-rich repeats (LRRs) of nucleotide-binding oligomerization domain containing 2 (NOD2) are associated with an increased risk for CD in many Caucasian populations,<sup>30–32</sup> but not in Japanese patients.<sup>33</sup> Therefore, it is of interest that increases in Agal-IgG levels are observed in Japanese and American IBD patients because of the clinical implications as a diagnostic marker, but also

as a reason to explore IgG glycosylation as a global defect in the pathogenesis of IBD.

An increase in serum agalactosyl IgG is also reported in other diseases such as RA,<sup>34</sup> SLE,<sup>35</sup> and tuberculosis.<sup>36</sup> In the present study we showed that Agal-IgG levels were significantly increased in patients with RA and SLE. Agal-IgG might be an effective serological marker for other immunological disorders such as SLE and RA. In addition, Agal-IgG levels in patients with CD are significantly higher than those with SLE and relatively higher than those with RA. Agalactosyl IgG seems to have different functions in each disease, because our recent studies show that the levels of anti-agalactosyl IgG antibodies are increased in the sera of RA<sup>37</sup> but not IBD patients.<sup>7</sup> Moreover, the lectin-complement pathway is activated through agalactosyl IgG in RA<sup>38</sup> but not IBD.<sup>8</sup> Therefore, the availability of an Agal-IgG lectin-EIA will help in translational studies to elucidate mechanisms through which agalactosyl IgG contributes to pathogenesis in different diseases.

In conclusion, the Agal-IgG lectin-EIA system for agalactosyl IgG may represent a novel biomarker assay for IBD. The presence of Agal-IgG in numerous autoimmune-inflammatory diseases has potential significance as a diagnostic marker that may fill important clinical needs, and may provide further information about pathogenesis.

#### ACKNOWLEDGMENTS

We thank Drs. Harumasa Yoshihara and Riichiro Nezu at Osaka Rosai Hospital and Dr. Satoshi Serada at Laboratory for Immune Signal, National Institute of Biomedical Innovation for providing serum samples.

#### REFERENCES

- Behm BW, Bickston SJ. Tumor necrosis factor- $\alpha$  antibody for maintenance of remission in Crohn's disease. *Cochrane Database Syst Rev*. 2008;CD006893.
- Prefontaine E, Macdonald JK, Sutherland LR. Azathioprine or 6-mercaptopurine for induction of remission in Crohn's disease. *Cochrane Database Syst Rev*. 2010;CD000545.
- Cannon RK, Kaiser AM, Ault GT, et al. Inflammatory bowel disease in the United States from 1998 to 2005: has infliximab affected surgical rates? *Am Surg*. 2009;75:976–980.
- Main J, McKenzie H, Yeaman GR, et al. Antibody to *Saccharomyces cerevisiae* (bakers' yeast) in Crohn's disease. *BMJ*. 1988;297:1105–1106.
- Quinton JF, Sendid B, Reuniaux D, et al. Anti-*Saccharomyces cerevisiae* mannan antibodies combined with antineutrophil cytoplasmic autoantibodies in inflammatory bowel disease: prevalence and diagnostic role. *Gut*. 1998;42:788–791.
- Benor S, Russell GH, Silver M, et al. Shortcomings of the inflammatory bowel disease Serology 7 panel. *Pediatrics*. 2010;125:1230–1236.
- Shinzaki S, Iijima H, Nakagawa T, et al. IgG oligosaccharide alterations are a novel diagnostic marker for disease activity and the clinical course of inflammatory bowel disease. *Am J Gastroenterol*. 2008;103:1173–1181.
- Nakajima S, Iijima H, Shinzaki S, et al. Functional analysis of agalactosyl IgG in inflammatory bowel disease patients. *Inflamm Bowel Dis*. 2011;17:927–936.
- Matsumoto H, Shinzaki S, Narisada M, et al. Clinical application of a lectin-antibody ELISA to measure fucosylated haptoglobin in sera of patients with pancreatic cancer. *Clin Chem Lab Med*. 2010;48:505–512.

- Hirabayashi J. Oligosaccharide microarrays for glycomics. *Trends Biotechnol*. 2003;21:141–143; discussion 143.
- Lenhard-Jones J. Classification of inflammatory bowel disease. *Scand J Gastroenterol Suppl*. 1989;170:2–6; discussion 16–19.
- Podolsky D. Inflammatory bowel disease (1). *N Engl J Med*. 1991;325:928–937.
- Podolsky D. Inflammatory bowel disease (2). *N Engl J Med*. 1991;325:1008–1016.
- Satsangi I, Silverberg MS, Vermeire S, et al. The Montreal classification of inflammatory bowel disease: controversies, consensus, and implications. *Gut*. 2006;55:749–753.
- Best W, Becktel J, Singleton J, et al. Development of a Crohn's disease activity index. National Cooperative Crohn's Disease Study. *Gastroenterology*. 1976;70:439–444.
- Rachmilewitz D. Coated mesalazine (5-aminosalicylic acid) versus sulphasalazine in the treatment of active ulcerative colitis: a randomised trial. *BMJ*. 1989;298:82–86.
- Hanauer SB, Feagan BG, Lichtenstein GR, et al. Maintenance infliximab for Crohn's disease: the ACCENT 1 randomised trial. *Lancet*. 2002;359:1541–1549.
- Kuno A, Uchiyama N, Koseki-Kuno S, et al. Evanescent-field fluorescence-assisted lectin microarray: a new strategy for glycan profiling. *Nat Methods*. 2005;2:851–856.
- Yamada Y, Hosoda T, Yoshizawa M, et al. Development and evaluation of the lectin-enzyme immune assay kit for detection of anti-agalactosyl IgG antibodies. *Clin Rep*. 1997;31:81–101.
- Beck JR, Shultz EK. The use of relative operating characteristic (ROC) curves in test performance evaluation. *Arch Pathol Lab Med*. 1986;110:13–20.
- Zweig MH, Campbell G. Receiver-operating characteristic (ROC) plots: a fundamental evaluation tool in clinical medicine. *Clin Chem*. 1993;39:561–577.
- Nakamura-Tsuruta S, Kominami J, Kamei M, et al. Comparative analysis by frontal affinity chromatography of oligosaccharide specificity of GlcNAc-binding lectins, Griffonia simplicifolia lectin-II (GSL-II) and Boletopsis leucomelas lectin (BLL). *J Biochem*. 2006;140:285–291.
- Nakamura-Tsuruta S, Kominami J, Kuno A, et al. Evidence that Agaricus bisporus agglutinin (ABA) has dual sugar-binding specificity. *Biochem Biophys Res Commun*. 2006;347:215–220.
- Kornfeld R, Ferris C. Interaction of immunoglobulin glycopeptides with concanavalin A. *J Biol Chem*. 1975;250:2614–2619.
- Presant CA, Kornfeld S. Characterization of the cell surface receptor for the Agaricus bisporus hemagglutinin. *J Biol Chem*. 1972;247:6937–6945.
- Chatterjee BP, Ahmed H, Uhlenbruck G, et al. Jackfruit (*Artocarpus integrifolia*) and the Agaricus mushroom lectin fit also to the so-called peanut receptor. *Helv Chim Acta*. 1985;148–158.
- Paulson JC, Blixt O, Collins BE. Sweet spots in functional glycomics. *Nat Chem Biol*. 2006;2:238–248.
- Huhn C, Selman MH, Ruhnauk LR, et al. IgG glycosylation analysis. *Proteomics*. 2009;9:882–913.
- Magro F, Portela F, Lago P, et al. Crohn's disease in a southern European country: Montreal classification and clinical activity. *Inflamm Bowel Dis*. 2009;15:1343–1350.
- Hampe J, Cuthbert A, Croucher PJ, et al. Association between insertion mutation in NOD2 gene and Crohn's disease in German and British populations. *Lancet*. 2001;357:1925–1928.
- Hugot JP, Chamaillard M, Zouali H, et al. Association of NOD2 leucine-rich repeat variants with susceptibility to Crohn's disease. *Nature*. 2001;411:599–603.
- Ogura Y, Bonen DK, Inohara N, et al. A frameshift mutation in NOD2 associated with susceptibility to Crohn's disease. *Nature*. 2001;411:603–606.
- Yamazaki K, Takazoe M, Tanaka T, et al. Absence of mutation in the NOD2/CARD15 gene among 483 Japanese patients with Crohn's disease. *J Hum Genet*. 2002;47:469–472.
- Parekh RB, Dwek RA, Sutton BJ, et al. Association of rheumatoid arthritis and primary osteoarthritis with changes in the glycosylation pattern of total serum IgG. *Nature*. 1985;316:452–457.
- Tomana M, Schrohlenhofer RE, Koopman WJ, et al. Abnormal glycosylation of serum IgG from patients with chronic inflammatory diseases. *Arthritis Rheum*. 1988;31:333–338.
- Parekh R, Iensenberg D, Rook G, et al. A comparative analysis of disease-associated changes in the galactosylation of serum IgG. *J Autoimmun*. 1989;2:101–114.
- Des H, Atsumi T, Fukushima Y, et al. Diagnostic value of antiagalactosyl IgG antibodies in rheumatoid arthritis. *Clin Rheumatol*. 2004;23:218–222.
- Malhotra R, Wormald MK, Rudd PM, et al. Glycosylation changes of IgG associated with rheumatoid arthritis can activate complement via the mannose-binding protein. *Nat Med*. 1995;1:237–243.

AQ1: Tables 2 and 3 cited out of order; switched.



## Plasma membrane proteomics identifies bone marrow stromal antigen 2 as a potential therapeutic target in endometrial cancer

Takuhei Yokoyama<sup>1,2</sup>, Takayuki Enomoto<sup>1</sup>, Satoshi Serada<sup>2</sup>, Akiko Morimoto<sup>1,2</sup>, Shinya Matsuzaki<sup>1,2</sup>, Yutaka Ueda<sup>1</sup>, Kiyoshi Yoshino<sup>1</sup>, Masami Fujita<sup>1</sup>, Satoru Kyo<sup>3</sup>, Kota Iwahori<sup>2</sup>, Minoru Fujimoto<sup>2</sup>, Tadashi Kimura<sup>1</sup> and Tetsuji Naka<sup>2</sup>

<sup>1</sup>Department of Obstetrics and Gynecology, Osaka University Graduate School of Medicine, Osaka, Japan

<sup>2</sup>Laboratory for Immune Signal, National Institute of Biomedical Innovation, Osaka, Japan

<sup>3</sup>Department of Obstetrics and Gynecology, Kanazawa University Graduate School of Medicine, Kanazawa, Japan

This report utilizes a novel proteomic method for discovering potential therapeutic targets in endometrial cancer. We used a biotinylation-based approach for cell-surface protein enrichment combined with isobaric tags for relative and absolute quantitation (iTRAQ) technology using nano liquid chromatography–tandem mass spectrometry analysis to identify specifically overexpressed proteins in endometrial cancer cells compared with normal endometrial cells. We identified a total of 272 proteins, including 11 plasma membrane proteins, whose expression increased more than twofold in at least four of seven endometrial cancer cell lines compared with a normal endometrial cell line. Overexpression of bone marrow stromal antigen 2 (BST2) was detected and the observation was supported by immunohistochemical analysis using clinical samples. The expression of BST2 was more characteristic of 118 endometrial cancer tissues compared with 59 normal endometrial tissues ( $p < 0.0001$ ). The therapeutic effect of an anti-BST2 antibody was studied both *in vitro* and *in vivo*. An anti-BST2 monoclonal antibody showed *in vitro* cytotoxicity in BST2-positive endometrial cancer cells *via* antibody-dependent cell-mediated cytotoxicity and complement-dependent cytotoxicity. In an *in vivo* xenograft model, anti-BST2 antibody treatment significantly inhibited tumor growth of BST2-positive endometrial cancer cells in an NK cell-dependent manner. The anti-BST2 antibody had a potent antitumor effect against endometrial cancer both *in vitro* and *in vivo*, indicating a strong potential for clinical use of anti-BST2 antibody for endometrial cancer treatment. The combination of biotinylation-based enrichment of cell-surface proteins and iTRAQ analysis should be a useful screening method for future discovery of potential therapeutic targets.

**Key words:** endometrial cancer, molecular target, plasma membrane, iTRAQ, BST2

**Abbreviations:** ADCC: antibody-dependent cell-mediated cytotoxicity; BST2: bone marrow stromal antigen 2; calcein-AM: calcein-acetoxymethyl ester; CDC: complement-dependent cytotoxicity; E/T ratio: effector to target ratio; FACS: fluorescence activated cell sorting; iTRAQ: isobaric tags for relative and absolute quantitation; LC: liquid chromatography; MS/MS: tandem mass spectrometry; NOD: nonobese diabetic; qRT-PCR: quantitative reverse transcription-PCR; SCID: severe combined immunodeficient; SCX: strong cation exchange; siRNA: small interfering RNA. Additional Supporting Information may be found in the online version of this article.

**Grant sponsors:** Grant-in-Aid for Scientific Research from the Japanese Ministry of Education, Science, Culture and Sports, Grant-in-Aid from the Ministry of Health, Labour and Welfare of Japan  
DOI: 10.1002/ijc.27679

**History:** Received 5 Mar 2012; Accepted 30 May 2012; Online 22 Jun 2012

**Correspondence to:** Tetsuji Naka, Laboratory for Immune Signal, National Institute of Biomedical Innovation, 7-6-8 Saitoasagi, Ibaraki City, Osaka 567-0085, Japan, Tel: +81-72-641-9843, Fax: +81-72-641-9837, E-mail: tnaka@nibio.go.jp

Anticancer monoclonal antibodies are a growing family of novel agents applied in the treatment regimens for hematopoietic and solid tumors. Antibody-based therapeutic agents against CD20 or Her2 have been successfully clinically developed and have significant therapeutic effects.<sup>1,2</sup> Tumor-associated antigens which are easily accessible from the tumor neovasculature are particularly attractive for intravenously-administered antibody-based therapeutic agents. During the last decade, several new technologies for high-throughput screening have identified many potential therapeutic targets. Thus far, no single approach or combination of methods has emerged as the preferred paradigm. It is clear that new tools and strategies are needed so that tumor-associated antigens can be screened efficiently.

Proteomic methods can now be tailored to search directly for targetable cell-surface proteins that distinguish cancer cells from normal cells. The complexity and concentration of individual proteins in the sample are crucial when performing proteomic analyses because abundant proteins, such as cytoskeletal proteins, may hinder the detection of low abundance proteins, such as plasma membrane proteins.<sup>3</sup> One way to enrich the potentially accessible cell-surface proteins is by whole cell protein tagging followed by affinity purification. A method for enrichment of such cell-surface proteins

**What's new?**

In this study, we have used a biotinylation-based approach for cell-surface protein enrichment combined with iTRAQ technology to identify and quantify membrane proteins which might represent potential therapeutic targets of endometrial cancer. A monoclonal antibody targeting BST2, one of the proteins identified in the iTRAQ analysis, have a potent antitumor effect against endometrial cancer both *in vitro* and *in vivo*, indicating a strong potential for clinical use of anti-BST2 antibody for endometrial cancer treatment.

*via* their biotinylation and affinity purification has been reported.<sup>4,5</sup> In most cases, concentrated cell-surface proteins are separated by SDS-PAGE and the enzymatically digested peptides are analyzed by mass spectrometry, while highly accurate quantitative data cannot be obtained by using this method. To acquire more quantitative information, stable isotope labeling using amino acids in cell culture (SILAC) based quantitative proteomics has been used, with high quantitative accuracy; however, the SILAC approach has the limitation that only a maximum of three samples can run in any single analysis.<sup>6,7</sup> Compared with SILAC, the more recently developed isobaric tags for relative and absolute quantitation (iTRAQ) technology has a distinct advantage regarding sample number handling capability in a single analysis, because iTRAQ can compare up to eight samples simultaneously.<sup>7,8</sup>

Endometrial cancer is the most common malignant tumor of the female genital tract. Its incidence varies among regions; it is overall the fourth most common malignancy in North America.<sup>9</sup> In general, the prognosis of these patients is excellent as the majority present with early-stage disease that is confined to the uterus at the time of diagnosis, which is followed by simple hysterectomy, leading to a 5-year survival rate of 84%.<sup>9</sup> Unfortunately, those women who present with recurrent or advanced-stage disease have a much poorer prognosis, with a median survival of less than a year.<sup>10</sup> To date, combination chemotherapy of cisplatin, doxorubicin, and paclitaxel has demonstrated the greatest efficacy.<sup>10-12</sup> However, these cytotoxic agents are associated with intolerable side effects and infrequent sustainable remission.<sup>11,12</sup> Thus, new and more effective targeted therapies for endometrial cancer are urgently needed. However, thus far the search for agents effective in the treatment of either recurrent or advanced endometrial cancer has been disappointing.<sup>12</sup>

Aiming for the identification of surface-accessible tumor antigens best suitable for antibody-based therapeutic intervention, it is important to analyze plasma membrane proteins known to be involved in endometrial cancer. For this purpose, we have utilized a novel proteomic technology by combining biotinylation-based approach for cell membrane enrichment and iTRAQ technology using nano liquid chromatography-tandem mass spectrometry (LC-MS/MS) analysis. In this study, one normal endometrial cell line (EM-E6/E7/TERT cells, immortalized normal endometrial cells) and seven endometrial cancer cell lines were used as a comparative model for studying the plasma membrane proteins related to endometrial cancer. Among 272 proteins identified

by iTRAQ analysis, bone marrow stromal antigen 2 (BST2) was investigated in more detail. By immunohistochemical analysis using actual clinical specimens, we found that the expression level of BST2 was significantly higher in endometrial cancer tissues compared with normal endometrial tissues. An anti-BST2 antibody showed potent antibody-dependent cell-mediated cytotoxicity (ADCC) and complement-dependent cytotoxicity (CDC) against BST2-positive endometrial cancer cells *in vitro*. In an *in vivo* xenograft model, anti-BST2 antibody treatment significantly inhibited tumor growth.

Taken together, our strategy of screening cell-surface tumor-specific antigens might be useful for identifying new therapeutic targets.

**Material and Methods****Cell lines and cultures**

We previously established an immortalized normal endometrial cell line (EM-E6/E7/TERT cells).<sup>13,14</sup> Nine human endometrial cancer cell lines (HEC-1, HEC-1A, HEC-6, HEC-88nu, HEC-108, HEC-116, HEC-251, SNG-II, and SNG-M cells) were obtained from the Japanese Collection of Research Bioresources (JCRB, Osaka, Japan), where they were tested and authenticated on June 30, 2011. The method used for testing was multiplexed PCR amplification of eight short tandem repeat loci (TH01, D5S818, D13S317, D7S820, D16S539, CSF1PO, vWA, and TPOX) and amelogenin was performed using the PowerPlex™16 System (Promega, Madison, WI). PCR-amplified fragments were analyzed with an ABI PRISM 310 Genetic Analyzer (Applied Biosystems, Foster City, CA). Then the fragments were typed based on allelic ladders. EM-E6/E7/TERT cells were maintained in a 1:1 mixture of DMEM and Ham's F12 medium (Wako Pure Chemical Industries, Osaka, Japan) supplemented with 10% FBS (HyClone Laboratories, Logan, UT) and 1% penicillin-streptomycin (Nacalai Tesque, Kyoto, Japan) at 37°C under a humidified atmosphere of 5% CO<sub>2</sub>. HEC-1, HEC-1A, HEC-6, HEC-88nu, HEC-108, HEC-116, and HEC-251 cells were maintained and propagated in DMEM (Wako Pure Chemical Industries) supplemented with 10% FBS and 1% penicillin-streptomycin. SNG-II and SNG-M cells were maintained in Ham's F12 (Invitrogen, Carlsbad, CA) with 10% FBS and 1% penicillin-streptomycin.

**Biotinylation of bovine serum albumin (BSA)**

BSA (30 μM) was biotinylated with a 100-fold molar excess of sulfo-succinimidyl 2-(biotinamido)-ethyl-1,3-dithiopropionate

(sulfo-NHS-SS-biotin; Pierce, Rockford, IL) and desalted as described previously.<sup>15</sup>

**Capture of cell-surface proteins**

To isolate cell-surface proteins, the normal endometrial cell line (EM-E6/E7/TERT cells) and seven endometrial cancer cell lines (HEC-1, HEC-1A, HEC-6, HEC-108, HEC-116, HEC-251, and SNG-II cells) were grown to approaching confluency (up to 90%) in three 15 cm dishes. Cells were washed three times with prewarmed PBS and then the cell-surface proteins were biotinylated for 15 min at room temperature with 15 ml of 500 μM sulfo-NHS-SS-biotin solution dissolved in PBS. The residual biotinylation reagent was quenched with 5 mM lysine for 5 min at room temperature. After biotinylation, the cells were washed with PBS twice, harvested by scraping, and collected by centrifugation (1,500 rpm, 4°C, 5 min). Detailed methods of extraction and purification of biotinylated cell-surface proteins are described in the Supporting Information Materials and Methods section.

**iTRAQ labeling**

Trypsin-digested peptides were dissolved in 5 μl of 9.8 M urea and 20 μl of IM TEAB. Samples were labeled with the iTRAQ reagent according to the manufacturer's protocol (Applied Biosystems). EM-E6/E7/TERT cells were labeled with iTRAQ reagent 113, HEC-1 cells with 114, HEC-1A cells with 115, HEC-6 cells with 116, HEC-108 cells with 117, HEC-116 cells with 118, HEC-251 cells with 119, and SNG-II cells with 121. The labeled peptide samples were then pooled and desalted with Sep-Pak Light C18 Cartridges (Waters, Manchester, UK) and peptides were dried in a centrifugal concentrator (Micro Vac MV-100, Tomy, Tokyo, Japan) before strong cation exchange (SCX) fractionation.

**SCX fractionation**

In order to remove excess unreacted iTRAQ reagent and to simplify the complexity of the peptide mixture, the labeled peptide mixtures were purified and fractionated using SCX column (SCX, PolySulfoethyl A column, 2.1 × 150 mm, 5 μm, 300 Å) on an Agilent 1200 HPLC system. Detailed information is provided in the Supporting Information Materials and Methods section.

**Mass spectrometric analysis**

Nano LC-MS/MS analyses were performed on an LTQ-Orbitrap XL (Thermo Fisher Scientific, Waltham, MA) equipped with a nano-ESI source and coupled to a Paradigm MG4 pump (Michrom Bioresources, Auburn, CA) and autosampler (HTC PAL, CTC Analytics, Zwingen, Switzerland). Detailed information is provided in the Supporting Information Materials and Methods section.

**iTRAQ data analysis**

Protein identification and quantification for iTRAQ analysis was carried out using Proteome Discoverer software (v. 1.1)

(Thermo Fisher Scientific) against Swiss Prot human protein database (SwissProt\_2011\_11, 533,049 entries). Taxonomy was set to *Homo sapiens* (20,326 entries) or mammalian (65,656 entries). Search parameters for peptide and MS/MS mass tolerance were 10 ppm and 0.8 Da, respectively, with allowance for two missed cleavages made from the trypsin digest. Carbamidomethylation (Cys) and iTRAQ8plex (Lys, N-terminal) were specified as static modifications, whereas CAMthiopropionyl (Lys, N-terminal), iTRAQ8plex (Tyr), and oxidation (Met) were specified as variable modifications in the database search. The false discovery rate of 1% was calculated by Proteome Discoverer based on a search against a corresponding randomized database. Relative protein abundances were calculated using the ratio of iTRAQ reporter ion in the MS/MS scan. For subcellular localization, all the proteins identified in this analysis were analyzed using the UniProtKB (available at: <http://www.uniprot.org/>) and Ingenuity Pathway Analysis software (Ingenuity Systems, Redwood City, CA).

**Quantitative reverse transcription-PCR (qRT-PCR) analysis**

To confirm the altered expression of BST2 in endometrial cancer, the normal endometrial cell line (EM-E6/E7/TERT cells) and nine endometrial cancer cell lines (HEC-1, HEC-1A, HEC-6, HEC-88nu, HEC-108, HEC-116, HEC-251, SNG-II, and SNG-M cells) were subjected to qRT-PCR. Total RNA was extracted using an RNeasy Mini Kit (Qiagen, Valencia, CA) and cDNAs were synthesized with a QuantiTect Reverse Transcription Kit (Qiagen), all according to the manufacturers' instructions. qRT-PCR was performed using SYBR Premix Ex taq (Takara Bio, Shiga, Japan) and an ABI 7900HT real-time PCR instrument (Applied Biosystems). β-Actin was used as a housekeeping gene for normalization of quantitative real-time PCR analysis. The primer sequences and the expected sizes of PCR products were as follows: BST2, forward primer 5'-GGAGGAGCTTGAGGGAGAG-3' and reverse primer 5'-CTCAGTCGCTCCACCTCTG-3', 75 bp; β-actin, forward primer 5'-AGCCTCGCCTTGCCGA-3' and reverse primer 5'-CTGGTGCCTGGGGCG-3', 174 bp. Relative quantitation of gene expression was performed using the standard curve method as outlined by Applied Biosystems. Experimental conditions were tested in triplicate and three independent experiments were performed.

**Fluorescence activated cell sorting (FACS) analysis**

Cells were washed twice in PBS (Nacalai Tesque) and detached with 0.02% EDTA solution (Nacalai Tesque). Cells were washed twice with cold FACS buffer (PBS supplemented with 1% FBS and 0.1% sodium azide) and then incubated with mouse anti-human BST2 antibody (Biolegend, San Diego, CA) at a 1:100 dilution and labeled with Alexa Fluor 488-labeled donkey anti-mouse IgG antibody (Invitrogen). Stained cells were analyzed using a FACS Canto cytometer (Becton Dickinson, Mountain View, CA) and the results were analyzed using FlowJo software (Tree Star, Stanford, CA).

### Patients and tissue samples

The formalin-fixed, paraffin-embedded tissue sections of 59 cases of normal endometrium and 118 cases of endometrial cancer were obtained from 177 patients who underwent surgical resections at Osaka University Hospital, Japan, between 1998 and 2007. Cases of normal endometrium were obtained from 59 patients who underwent simple hysterectomy for benign indications such as leiomyoma and uterine prolapse. Histological features of the tissues were reviewed by board-certified pathologists. The degree of histological differentiation and surgical pathological staging of 118 cases of endometrial cancer were assigned according to the 1988 recommendations of International Federation of Gynecology and Obstetrics. A summary of clinicopathological information for these patients is shown in Supporting Information Table S1. Written informed consent was obtained for all the cases and the experimental protocol was approved by the ethics committees of Osaka University and National Institute of Biomedical Innovation.

### Immunohistochemistry

Sections were prepared from formalin-fixed, paraffin-embedded tissue specimens, deparaffinized, and rehydrated in graded alcohols. Immunohistochemical staining for BST2 was performed using the avidin-biotin-peroxidase complex (ABC) method using a rabbit polyclonal anti-BST2 antibody (Sigma-Aldrich, St. Louis, MO) and the Vectastain ABC kit (Vector Laboratories, Burlingame, CA) according to the manufacturer's protocol. Immunostained sections were photographed with an Olympus FSX100 (Olympus, Tokyo, Japan). Detailed information is provided in the Supporting Information Materials and Methods section.

### Evaluation of immunohistostaining

Immunostainings were scored according to the intensity of the staining (no staining = 0, weak staining = 1, moderate staining = 2, strong staining = 3) and the extent of stained cells (0–9% = 0, 10–40% = 1, 41–70% = 2, 71–100% = 3). The final immunohistochemistry (IHC) score was determined by multiplying the intensity score (0, 1, 2, or 3) with the positivity score (0, 1, 2, or 3), resulting in a maximum score of 9. Three independent gynecologic oncologists (Y.U., K.Y., and M.F.), blinded to the histological data, analyzed the stained sections using an Olympus BH2 microscope (Olympus). In case of disagreement, the staining results were re-evaluated by careful discussion until a consensus was reached.

### Cell proliferation assay

Endometrial cancer cells plated in 96-well plates (1,000 cells per well) were grown in their respective media for 24, 48, or 72 hr after the addition of antibody or small interfering RNA (siRNA) transfection. At each time point, cell proliferation was assessed by a WST-8 assay according to the manufacturer's protocol (Nacalai Tesque). Detailed information for these assays can be found in the Supporting Information Materials and Methods section.

### ADCC assay

ADCC was measured by calcein-acetoxymethyl ester (calcein-AM) release assay, with sensitivity similar to the traditional  $^{51}\text{Cr}$  release assay.<sup>16,17</sup> Detailed information for this assay can be found in the Supporting Information Materials and Methods section.

### CDC assay

CDC was evaluated using a  $^{51}\text{Cr}$  release assay.<sup>18</sup> Detailed information for this assay can be found in the Supporting Information and Methods section.

### Tumor xenograft and antibody therapy

Healthy female severe combined immunodeficient (SCID) and nonobese diabetic (NOD)/SCID mice at 8 weeks of age were obtained from Charles River Japan (Yokohama, Japan) and maintained in a specific pathogen-free facility. For subcutaneous xenograft experiments, SCID mice were inoculated subcutaneously with  $5 \times 10^6$  HEC-88nu or SNG-II cells in a total volume of 50  $\mu\text{l}$  of 1/1 (v/v) PBS/Matrigel (Becton Dickinson) into the abdomen. NOD/SCID mice were inoculated with  $5 \times 10^6$  HEC-88nu cells. PBS, isotype control (mouse IgG2a $\kappa$ , Sigma-Aldrich), or mouse anti-human BST2 antibody (clone 1B4; Chugai Pharmaceutical) was administered intraperitoneally at a dose of 5 mg/kg (SNG-II) or 10 mg/kg (HEC-88nu) in 400  $\mu\text{l}$  of PBS. Six mice were used per group. The first dose was given on day 4 (SNG-II) or 9 (HEC-88nu) and continued twice weekly for 4 weeks. Tumors were measured twice weekly from days 4 (SNG-II) or 9 (HEC-88nu) using vernier calipers throughout the study. Tumor volumes were calculated using the following formula: tumor volume ( $\text{mm}^3$ ) = length  $\times$  width  $\times$  height. After 8 (HEC-88nu) or 12 (SNG-II) weeks, tumors were resected and weighted. All animal experiments were conducted according to the institutional ethical guidelines for animal experimentation of the National Institute of Biomedical Innovation.

### Statistical analysis

For immunohistochemistry, statistical significance of difference between normal endometrium and endometrial cancer was analyzed by the nonparametric Mann-Whitney *U* test. Differences in the *in vitro* cytotoxic assay were determined by using the Kruskal-Wallis test followed by the Steel procedure. For all subcutaneous tumor comparisons, groups were analyzed using the Kruskal-Wallis test followed by the Steel-Dwass procedure.

## Results

### Protein expression profiles in normal endometrium and endometrial cancer

To identify potential therapeutic targets of endometrial cancer, we performed comparative protein expression profiling between normal endometrium (EM-E6/E7/TERT cells) and

endometrial cancer (HEC-1, HEC-1A, HEC-6, HEC-108, HEC-116, HEC-251, and SNG-II cells) at the cell surface level. We identified a total of 272 proteins by a biotinylation-based approach for cell membrane enrichment combined with iTRAQ technology using nano LC-MS/MS analysis. The complete list of all the proteins identified is shown in Supporting Information Table S2. The list of proteins identified with single peptide is provided in Supporting Information Table S3. MS/MS spectra of all single-peptide-based assignments with masses detected as well as fragment assignments are presented in Supporting Information Table S4. The raw MS data of this analysis is publicly available for download from PeptideAtlas (available at: <http://www.peptideatlas.org/PASS/PASS00032>). To correct the error of quantitation during chromatographic procedures, we added the equivalent moles of the sulfo-NHS-SS-biotin labeled BSA into the each sample as an internal standard. The iTRAQ ratio of BSA (0.873 to 1.131, Supporting Information Table S3) was used for the correction of quantitation information accurately. According to the annotation from UniprotKB and Ingenuity Pathway Analysis, 139 proteins (51% of the identified proteins) were located in the plasma membrane (Fig. 1a). Among these 139 plasma membrane proteins identified, 11 proteins were increased more than twofold in at least four of seven endometrial cancer cell lines compared with the normal endometrial cell line (Table 1). As expected, neural cell adhesion molecule 1, a plasma membrane protein previously known to be overexpressed in endometrial cancer, was identified again. Interestingly, BST2 was found to show one of the most significant differences in expression between normal endometrial cells and endometrial cancer cells, making it a prime target.

### Confirmatory studies by qRT-PCR and FACS

To confirm the altered expression of BST2 in endometrial cancer, we first evaluated its transcripts by qRT-PCR in the normal endometrial cell line (EM-E6/E7/TERT cells) and nine endometrial cancer cell lines (HEC-1, HEC-1A, HEC-6, HEC-88nu, HEC-108, HEC-116, HEC-251, SNG-II, and SNG-M cells). BST2 mRNA expression was clearly detected in seven of the nine endometrial cancer cell lines, while the normal endometrial cell line showed no detectable expression of BST2 transcripts (Fig. 1b).

We then evaluated the expression of BST2 at the protein level and confirmed the surface localization of BST2 by FACS analysis. Protein expression of BST2 was very weak in EM-E6/E7/TERT cells. In contrast, a considerably higher level of BST2 protein expression was detected in six of the nine endometrial cancer cell lines on the cell surface (Fig. 1c). Together our data demonstrate that BST2 was overexpressed in endometrial cancer cells at both the mRNA and protein level; this was consistent with our iTRAQ analysis.

### Validation study by IHC

As a validation study, immunohistochemical analyses were performed by examination of the BST2 expression pattern

in paraffin-embedded tissue samples (Supporting Information Table S1). Representative immunohistochemical staining of BST2 in tissue sections from patients revealed intense BST2 staining in endometrial cancer compared with normal endometrium (Fig. 2a). In addition, immunohistochemical analyses showed membranous immunoreactivity in endometrial cancer cells, indicating that the localization of BST2 was at cell surface. We observed significantly stronger positive staining of BST2 in tissue sections from patients with endometrial cancer compared with normal endometrium ( $p < 0.0001$ ) (Fig. 2b). In 118 endometrial cancer specimens, moderately to strongly positive staining (IHC score = 3–9) was detected in 71.2% of specimens (84 of 118), whereas only 1.7% (1 of 59) were positive in the normal endometrial specimens. There were no significant differences in BST2 immunohistochemical staining among endometrial cancer tissues according to their degree of histological differentiation or surgical pathological staging ( $p = 0.77$  and  $0.06$ , respectively, by the Kruskal-Wallis test). There were no significant differences in BST2 staining among normal proliferative-phase, secretory-phase, and atrophic endometrium ( $p = 0.82$  by the Kruskal-Wallis test). These results indicate that BST2 was overexpressed on the cell surface of endometrial cancer tissues much more frequently than in normal endometrium, raising the possibility that BST2 might represent a potential therapeutic target.

### BST2-siRNA and anti-BST2 antibody treatment *in vitro*

To examine whether the BST2 expression contributes to cell proliferation of endometrial cancer cells, the effect of BST2-siRNA treatment in four of the endometrial cancer cell lines expressing BST2 (HEC-6, HEC-88nu, HEC-116, and SNG-II cells) was evaluated using the WST-8 assay. To ensure silencing efficiency, BST2 expression was analyzed by FACS analysis after 48 hr of siRNA transfection. The two siRNAs targeting BST2 (Hs\_BST2\_1 and Hs\_BST2\_5) had a similar silencing effect on the protein level (Supporting Information Fig. S1). There were no significant differences in cell proliferation among BST2-siRNA and control-siRNA treated cells (Fig. 3a). Similarly, anti-BST2 antibody treatment did not affect *in vitro* cell proliferation (Fig. 3b).

We subsequently examined whether an anti-BST2 antibody can induce ADCC among endometrial cancer cells using the calcein-AM release assay. To study the specificity of anti-BST2 antibody-mediated ADCC against BST2-expressing target cells, an ADCC assay was performed using a BST2-expressing endometrial cancer cell line (HEC-88nu cells) and a BST2-negative cell line (HEC-1 cells). As shown in Figure 3c, HEC-88nu cells treated with the anti-BST2 antibody showed specific lysis *via* ADCC ( $p = 0.045$ ), whereas the anti-BST2 antibody showed no lytic activity against HEC-1 cells.

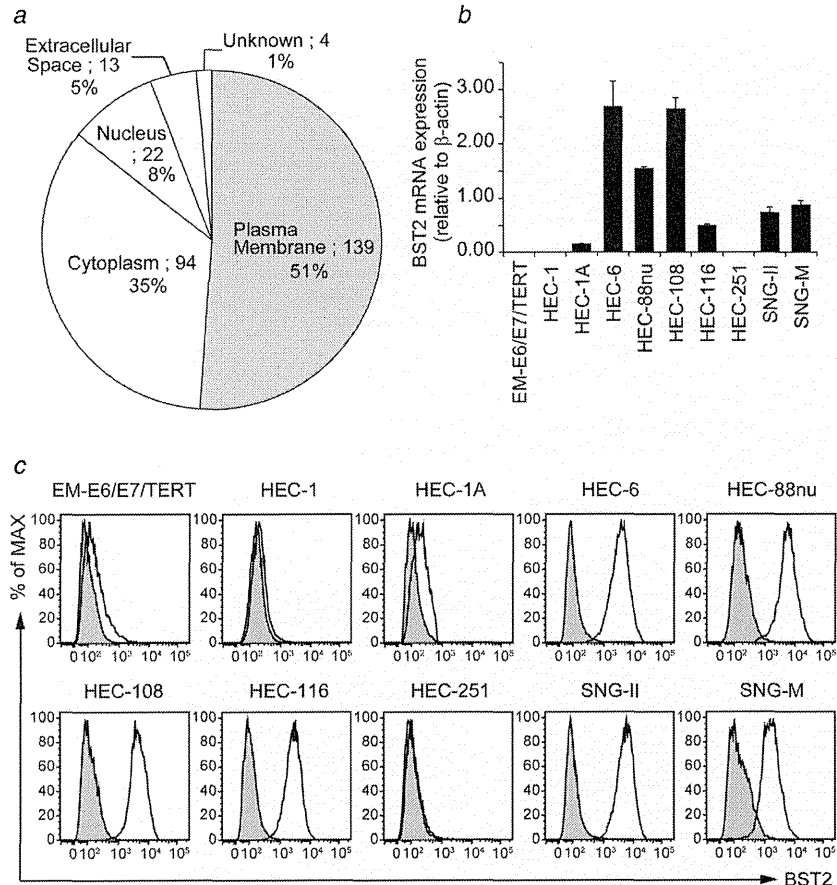


**Figure 1.** (a) Subcellular localization of the identified 272 proteins analyzed by UniprotKB and Ingenuity Pathway Analysis. (b) Confirmation of ITRAQ results by qRT-PCR. qRT-PCR was used to quantify BST2 mRNA;  $\beta$ -actin was used as the internal control. Data are mean  $\pm$  SEM of three independent experiments, each performed in triplicate. BST2 mRNA expression was not detected in the normal endometrial cell line (EM-E6/E7/TERT cells), but seven of nine endometrial cancer cell lines exhibited positive expression of BST2 mRNA. (c) Confirmation of ITRAQ results by FACS analysis. The shaded histogram profile indicates the isotype control, and the open histogram indicates the anti-BST2 antibody staining results.

We also examined CDC exhibited by the anti-BST2 antibody. Figure 3d shows that the BST2-expressing endometrial cancer cell line (HEC-88nu cells), but not the BST2-negative cell line (HEC-1 cells), was sensitive to CDC ( $p = 0.045$ ).

**Therapeutic effect of the anti-BST2 antibody *in vivo***

To evaluate the therapeutic efficacy of anti-BST2 antibody therapy, *in vivo* studies were performed using an endometrial cancer xenograft model. SCID mice injected with either

HEC-88nu or SNG-II cells (BST2-expressing endometrial cancer cell lines) were assigned to one of three treatment groups ( $n = 6$  per group): (i) PBS; (ii) isotype control; (iii) anti-BST2 antibody, 5 mg/kg (SNG-II) or 10 mg/kg (HEC-88nu) twice weekly. Although the tumors of all mice were approximately equal in initial volumes, significant differences in tumor growth were observed during the study, as illustrated by the tumor growth curve in Figure 4a. All mice were sacrificed on days 61 (HEC-88nu) or 85 (SNG-II) post-tumor inoculation. The tumors of the anti-BST2 antibody treatment group were markedly smaller than that of the PBS and control IgG treatment groups (Fig. 4b). The tumor weights of the anti-BST2 antibody treatment group were significantly decreased compared with the PBS and control IgG treatment groups, whereas there was no statistical difference between the PBS and control IgG treatment groups at the termination of the experiment (Fig. 4c).

Once we had established a proof of principle that the anti-BST2 antibody can inhibit tumor growth, we then sought to identify mechanisms by which the anti-BST2 antibody acts on tumor cells. Anti-BST2 antibody treatment showed no significant therapeutic effect in identically treated NOD/SCID mice, with anti-BST2 antibody treated mice developing tumors at virtually the same rate as PBS and control IgG treated mice (Fig. 5).

**Discussion**

Our study focused on a novel biotechnological method we found to be useful for identifying tumor-associated cell-surface antigens differentially expressed in cancer cells with respect to corresponding normal cells. The ideal expression pattern of a tumor-specific antigen for antibody therapy is that it should be abundant and homogeneous on the surface of cancer cells, and absent from normal tissue.<sup>19</sup> Such targets can be experimentally identified at different molecular levels, such as DNA, RNA, and protein.

DNA microarray technologies have led to the identification of genes that are dysregulated in cancer cells when compared with normal cells.<sup>20,21</sup> However, DNA arrays measure only the changes at the mRNA level, and this is not always translated to corresponding changes at the protein level, leading to many false positives and missed positives. The use of mRNA expression patterns by themselves is often insufficient for understanding the expression of protein products, as additional post-translational mechanisms, including protein translation, post-translational modification, and degradation, may influence the level of a protein and its antigenic epitopes.<sup>22,23</sup> In addition, effective induction of ADCC or CDC mediated by a therapeutic antibody requires abundant expression of cell-surface proteins specifically on the cancer cells,<sup>24,25</sup> providing a compelling rationale for a more direct analysis of gene expression at the protein level by proteomic methods.

The intensity of individual proteins in the sample is crucial when performing proteomic analyses, as larger amounts

**Cancer Therapy**

**Table 1.** Plasma membrane proteins overexpressed in endometrial cancer cells

Accession number	Protein name	No. peptides used for identification	ITRAQ ratio									
			HEC-1	HEC-1A	HEC-6	HEC-108	HEC-116	HEC-251	SNG-II	SNG-M		
Q14672	Disintegrin and metalloprotease domain-containing protein 10	5	1.670	1.271	2.032	3.175	2.824	3.958	1.364			
P11279	Lysosome-associated membrane glycoprotein 1	1	0.398	3.017	5.745	8.722	4.307	5.239	1.727			
P25942	Tumor necrosis factor receptor superfamily member 5	2	2.518	5.353	7.796	6.438	8.526	2.747	n.d.			
P31431	Syndecan-4	5	n.d.	0.949	1.644	2.905	4.396	8.121				
P32004	Neural cell adhesion molecule L1	26	1.211	0.905	2.171	9.025	2.603	13.756	4.283			
P50895	Basal cell adhesion molecule	15	0.692	0.876	5.378	2.493	2.363	3.936	2.864			
P78310	Coxsackievirus and adenovirus receptor	3	1.773	3.140	5.228	16.042	4.507	3.265	3.256			
Q10589	Bone marrow stromal antigen 2	2	n.d.	6.438	85.276	94.318	87.278	3.435	38.946			
Q14126	Desmoglein-2	9	2.360	3.199	1.912	2.827	5.286	2.542	4.637			
Q9H5V8	CUB domain-containing protein 1	2	0.907	2.234	11.680	3.508	11.603	8.623	17.020			
Q9Y624	Junctional adhesion molecule A	1	4.374	17.088	25.645	47.784	23.673	77.025	18.523			

The ITRAQ ratios were calculated comparing the endometrial cancer cells' ITRAQ signal divided by the normal endometrial cells' ITRAQ signal. Proteins overexpressed more than twofold in at least four cell lines are listed. Abbreviations: n.d. = Not detected.

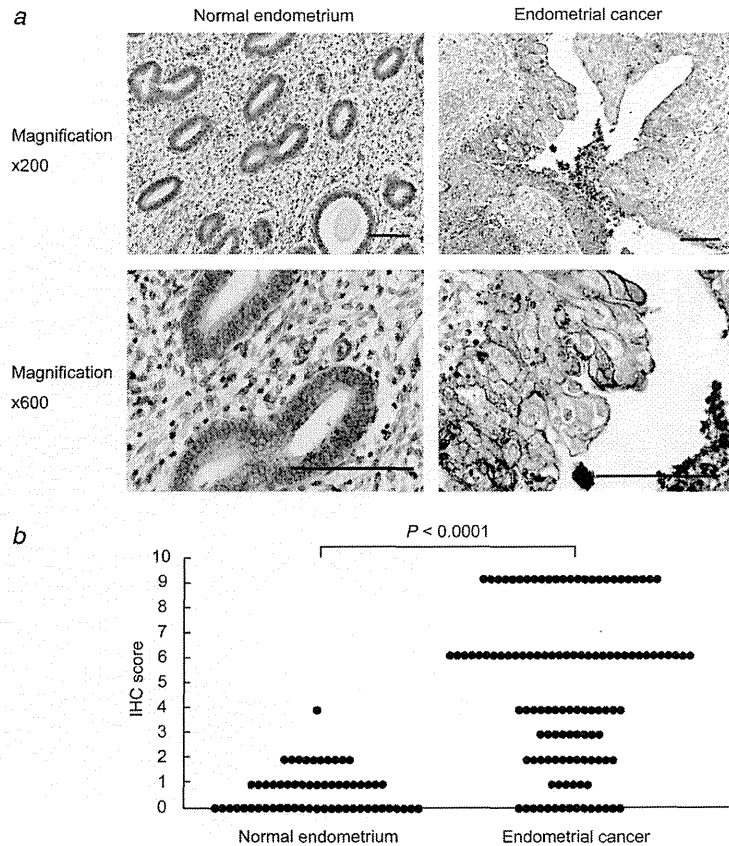


**Figure 2.** (a) Representative immunohistochemical staining for BST2 in normal endometrium and endometrial cancer specimens. Immunostained sections were counterstained with hematoxylin and photographed with an Olympus FSX100 (Olympus). The expression of BST2 was negative in normal endometrium, whereas endometrial cancer showed strong membranous reactivity for BST2. Scale bar, 100  $\mu$ m. (b) BST2 immunoreactivity in normal endometrial tissues and endometrial cancer tissues. The expression of BST2 was increased in endometrial cancer, with significant difference ( $p < 0.0001$ ). IHC score = intensity score (0, 1, 2, or 3)  $\times$  positivity score (0, 1, 2, or 3).

of some proteins may hinder the detection of less abundant proteins, such as cell-surface membrane proteins. As such, enrichment of plasma membrane proteins is an important initial step. Physical isolation of membrane proteins using centrifugation and/or chemical extraction are well-described methods.<sup>26,27</sup> However, these techniques fail to isolate only the cell-surface membrane proteins and usually provide

extracts that consist of all the membrane structures, including those inside the cell (e.g., endoplasmic reticulum, Golgi apparatus, and mitochondrial membranes). The proteins that are found inside the cell will most likely not be accessible to the systemically delivered antibodies and hence do not represent a group of interest for discovery of targetable molecules. Another way to enrich specifically the potentially accessible

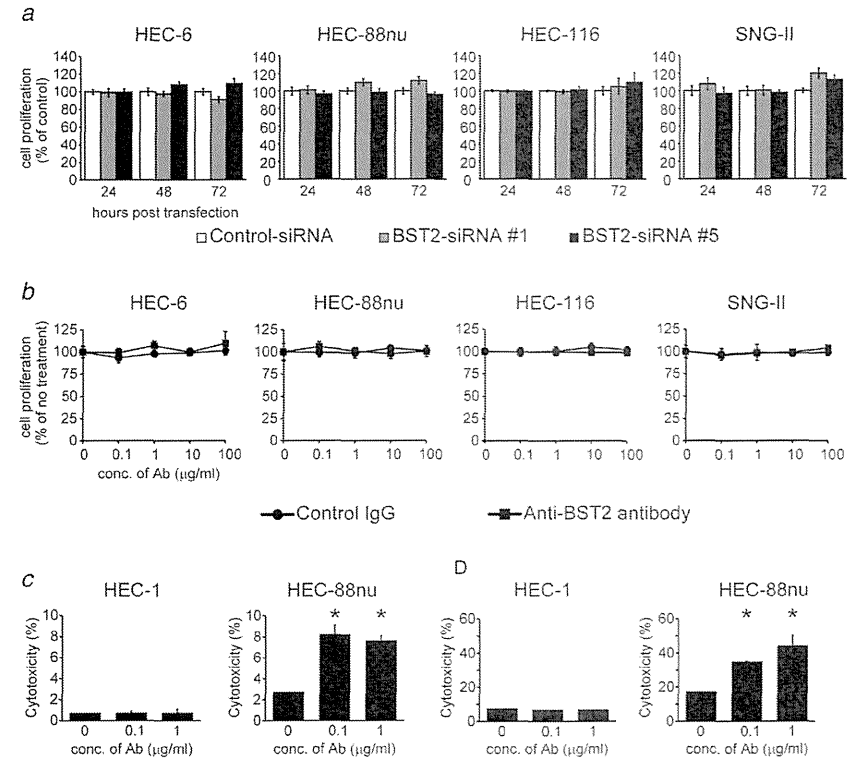


**Figure 3.** *In vitro* growth assay of endometrial cancer cells treated with BST2-siRNA (a) or anti-BST2 antibody (b). HEC-6, HEC-88nu, HEC-116, and SNG-II cells are BST2-positive endometrial cancer cell lines. (a) A total of 1,000 cells were plated in each well of 96-well plates and then siRNA was transfected. Cell proliferation was assessed at 24, 48, and 72 hr using a WST-8 assay. Values were normalized to control-siRNA treated cells. There were no significant differences in cell proliferation among BST2-siRNA and control-siRNA treated cells. (b) Anti-BST2 antibody or isotype-control IgG (final concentrations of 0.1, 1, 10, or 100  $\mu$ g/ml) were added to 1,000 cells/well in 96-well plates. Cell proliferation was assessed at 72 hr using the WST-8 assay. Values were normalized to untreated cells. Anti-BST2 antibody had no direct cytotoxic effect on endometrial cancer cells *in vitro*. (c), ADCC activity of anti-BST2 antibody. Calcein-labeled HEC-1 (BST2-negative) and HEC-88nu (BST2-positive) cells were incubated with bone marrow-derived lymphokine-activated killer cells at an E/T ratio of 50 in the presence of 0, 0.1, or 1.0  $\mu$ g/ml anti-BST2 antibody. (d) CDC activity of anti-BST2 antibody. <sup>51</sup>Cr-labeled HEC-1 (BST2-negative) and HEC-88nu (BST2-positive) cells were incubated with 12.5% baby rabbit complement in the presence of 0, 0.1, or 1.0  $\mu$ g/ml anti-BST2 antibody. Anti-BST2 antibody had ADCC and CDC activity against HEC-88nu cells (BST2-expressing endometrial cancer cell line). \* $p = 0.045$ .

cell-surface proteins involves conjugating membrane proteins with the small molecule biotin and using the receptor streptavidin to extract the labeled proteins.<sup>28,29</sup>

In this study, we quantitatively analyzed the plasma membrane profiles comparing normal endometrium and endometrial cancer using a biotinylation-based approach for cell membrane enrichment combined with iTRAQ technology

using nano LC-MS/MS analysis. While quantitative membrane proteomic approaches combining biotin labeling followed by enrichment of cell surface membrane proteins by avidin-beads and SILAC technology or spectral counting were already reported,<sup>28,30</sup> we demonstrated that iTRAQ approach is also an alternative method, suitable for the quantitative analysis of the cell surface membrane proteins.

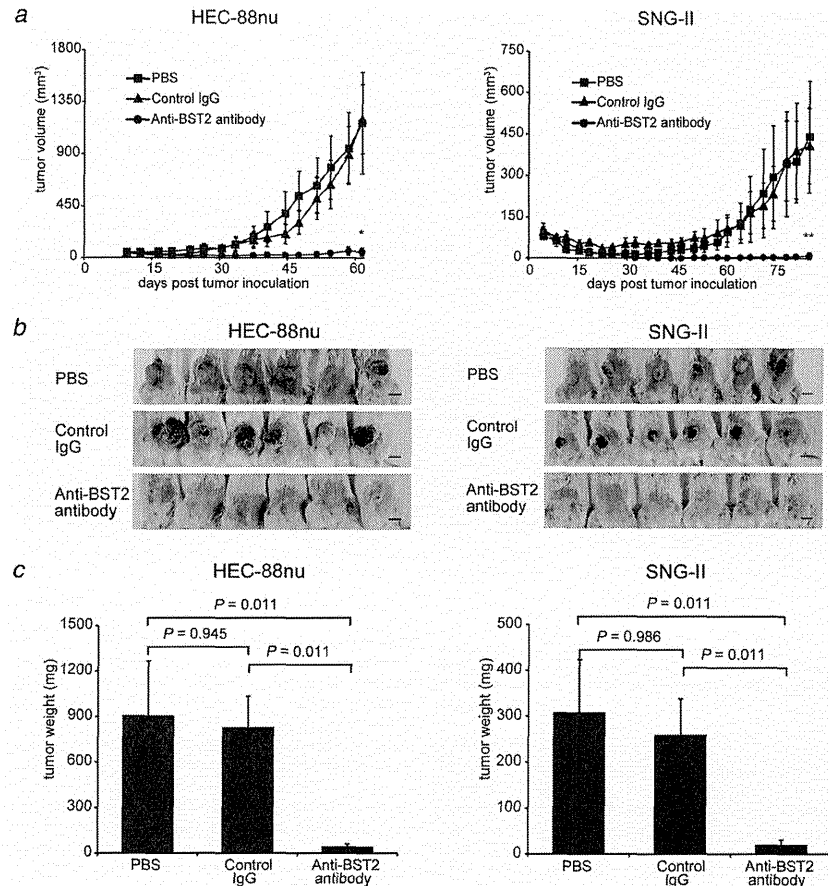


**Figure 4.** *In vivo* therapeutic effect of anti-BST2 antibody on endometrial cancer growth. SCID mice inoculated with HEC-88nu or SNG-II cell lines (both are BST2-expressing endometrial cancer cell lines) received PBS, control IgG, or anti-BST2 antibody twice a week for 4 weeks from days 4 (SNG-II) or 9 (HEC-88nu) post-tumor inoculation. (a) Time-course of tumor volume change. Tumor volumes were measured twice a week and calculated as the product of length, width, and height. The mean volume  $\pm$  SD of six tumors in each group is shown. Anti-BST2 antibody treatment resulted in significantly decreased tumor growth compared with the other control groups (PBS and control IgG) at the termination of the experiment. \* $p = 0.0110$ , \*\* $p = 0.0108$ . (b) Mice at the end of the experiment. Scale bar, 1 cm. (c) Tumor weight at autopsy. After 4 (HEC-88nu) or 8 (SNG-II) weeks of observation following treatment, tumors were removed and weighed. Their weights were significantly different between the experimental (anti-BST2 antibody) group and the control (PBS and control IgG) groups ( $p = 0.011$ ).

In total, we identified 272 proteins, 139 of which (51%) were found to be cell-surface proteins. Given that global genomic analysis predicts that 20 to 30% of all open reading

frames encode integral membrane proteins,<sup>31</sup> our results indicate that the membrane proteins were moderately enriched by our sample preparation strategy.

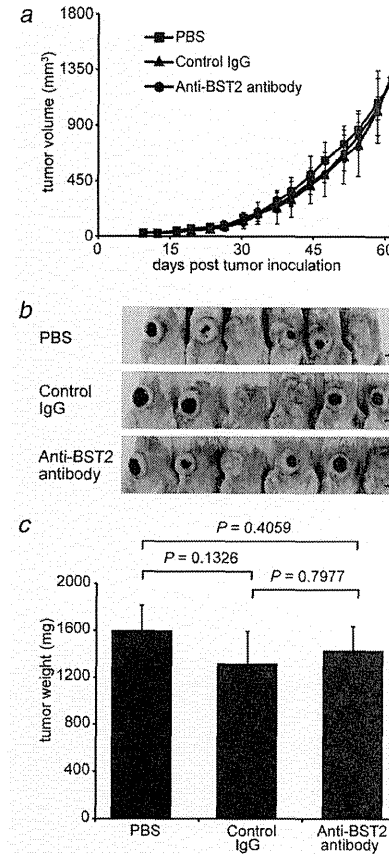


**Figure 5.** Natural killer cells are required for antitumor activity of anti-BST2 antibody *in vivo*. NOD/SCID mice inoculated with HEC-88nu cells (BST2-expressing endometrial cancer cell line) received PBS, control IgG, or anti-BST2 antibody twice a week for 4 weeks from day 9 post-tumor inoculation. (a) Time-course of tumor volume change. Tumor volumes were measured twice a week and calculated as the product of length, width, and height. The mean volume  $\pm$  SD of six tumors in each group is shown. There were no significant differences in tumor volumes among PBS, control IgG, and anti-BST2 antibody groups at the termination of the experiment. \* $p = 0.9769$ . (b) Mice at the end of the experiment. Scale bar, 1 cm. (c) Tumor weight at autopsy. After 4 weeks of observation following treatment, tumors were removed and weighed. There were no significant differences in tumor weights among the three groups.

Eleven proteins were annotated as unique membrane proteins whose expression was specifically up-regulated in endometrial cancer (Table 1). These proteins included several reported markers for prediction of clinical outcome (neural cell adhesion molecule L1 and CUB domain-containing protein 1), suggesting a certain amount of robustness for our methodology of identifying tumor-associated antigens.<sup>32,33</sup> In the present study, BST2 was further validated as a potential therapeutic target for endometrial cancer, because BST2 showed one of the most significant differences between normal endometrium and endometrial cancer (a 10-fold up-regulation was shown in four of seven endometrial cancer cell lines compared with the normal endometrial cell line) and has been reported to be overexpressed in endometrial cancer using genome-wide gene expression profiling.<sup>21</sup> In future work, we would like to characterize other novel candidates for developing new therapeutic agents.

BST2 (also termed CD317, tetherin, or HM1.24) was originally identified as a Type II membrane glycoprotein with an unusual topology (one-pass transmembrane domain and C-terminal glycosylphosphatidylinositol anchor) that is preferentially overexpressed on multiple myeloma cells.<sup>34,35</sup> More recently, BST2 has also been proposed as a tumor-associated antigen expressed in some human cancer cell lines.<sup>36-38</sup> However, BST2 is an interferon-induced protein and inflammatory cytokines such as interleukin-6 and tumor necrosis factor- $\alpha$  might also induce its expression.<sup>35</sup> Furthermore, BST2 has been found to block the release of enveloped virus particles (e.g., HIV-1, Marburg virus, and Ebola virus) and may therefore be an important component of the antiviral innate immune defense.<sup>39,40</sup> Future research should further explore the role of BST2 in inflammatory diseases.

To our knowledge, protein expression of BST2 in endometrial cancer has not been described before. Our results are the first to show that BST2 is significantly overexpressed in endometrial cancer compared with normal endometrium. The degree of histological differentiation and surgical pathological staging showed no significant correlation with expression of BST2. Given the almost ubiquitous expression of BST2 in endometrial cancer, BST2 might have some value acting as a potential molecular therapeutic target.<sup>19</sup> In this study, we demonstrated that the administration of the anti-BST2 antibody reduced the growth of BST2-positive endometrial cancer cells in SCID mice. The suppressive effects on tumor growth were observed in two cell lines. In principle, the putative mechanisms of monoclonal antibody-based cancer therapy can be classified into two categories.<sup>41,42</sup> One mechanism is direct action to block the function of target signaling molecules or receptors, or stimulate apoptosis. It has been reported that BST2 gene is one of the important activators of the NF- $\kappa$ B pathway,<sup>43</sup> suggesting that the signaling from BST2 antigen affects the biological responses of BST2-expressing cells. However, silencing of BST2 expression by siRNA transfection did not alter its cell proliferation, and the anti-BST2 antibody had no direct cytotoxic effect on